Original Article

Mineralogy, Fluid Inclusion, and Hydrogen and Oxygen Isotope Studies of the Intrusion-Related Yangla Cu Deposit in the Sanjiang Region, SW China: Implications for Metallogenesis and Deposit Type

Li-Juan Du,[1,2] Bo Li,[3] Zhi-Long Huang,[2] Jun Chen,[2] Jia-Xi Zhou,[2] Guo-Fu Zou[4] and Zai-Fei Yan[2]

[1]*College of Resources and Environmental Engineering, Guizhou University,* [2]*State Key Laboratory of Ore Deposit Geochemistry, Institute of Geochemistry, Chinese Academy of Sciences, Guiyang,* [3]*Faculty of Land Resources Engineering, Kunming University of Science and Technology and* [4]*Yunnan Copper Group, Kunming Prospecting Design Inst China Nonferrous, Kunming, China*

Abstract

The Yangla deposit is an intrusion-related Cu deposit in the Jinshajiang tectonic belt (eastern Sanjiang region, SW China). Despite extensive studies that have been conducted on this deposit, the relationship between the granitic magma and Cu mineralization is still unclear, and hence, the genesis is debated. To answer this question, we conducted an integrated study of mineralogy, fluid inclusions (FIs), and hydrogen and oxygen (H-O) isotopes. Three mineralization stages were identified based on the ore textures, alteration zonation, and crosscutting relationships: (i) pre-ore prograde skarn (stage I), with the garnet and pyroxene dominated by andradite and diopside, respectively; (ii) syn-ore retrograde alteration (stage II), which is subdivided into the early syn-ore stage (stage IIa) marked by retrograde hydrated mineral assemblages and significant Fe-Cu-Mo-Pb-Zn sulfide mineralization, and the late syn-ore stage (stage IIb) featured by quartz-calcite veins; and (iii) late supergene mineralization (stage III), which is characterized by secondary azurite and malachite. These results of mineralogy, FIs, and H-O isotopes indicate that: (i) Cu mineralization has a close temporal, spatial, and genetic relationship with skarn alteration; (ii) the ore fluids were magmatic dominated with late-stage meteoric water incursion; and (iii) Type-S (halite-bearing) and Type-V (vapor-rich) FIs coexisted in garnet and clinopyroxene of stage I, indicating that fluid boiling might have occurred during this stage. From stage I to stage IIa, the FI type transformed from Type-S + Type-V + Type-L (liquid-rich) to Type-V + Type-L with the conduct of mineralization and was accompanied by the disappearance of Type-S, and homogenization temperature and salinity also tended to decrease dramatically, which may be caused by the deposition of skarn minerals. At stage IIa, boiling of the ore fluids still continued due to the change from lithostatic to hydrostatic pressure, which triggered the precipitation of abundant quartz-Cu-Mo-Fe sulfides. Furthermore, fluid mixing between a high-temperature magmatic fluid and a low-temperature meteoric water might cause a considerable drop in temperature and the deposition of Cu-bearing quartz/calcite veins during stage IIb. Hence, we consider the Yangla deposit to be of a skarn type, genetically related to the Mesozoic magmatism in the Sanjiang region.

Keywords: fluid inclusions, fluid source and evolution, H-O isotopes, Sanjiang region (SW China), Yangla Cu skarn deposit.

1. Introduction

The Sanjiang (*Chinese:* "three rivers," referring to the Jinshajiang, Lancangjiang, and Nujiang rivers) region in SW China is a key component of the eastern Tethyan-Himalayan metallogenic belt. It is one of the prime polymetallic terranes in China and contains numerous important precious/base metal deposits (Fig. 1a) (Mo *et al.,* 1993; Hou *et al.,* 2007; Zaw *et al.,* 2007; Deng *et al.,* 2014a; Deng *et al.,* 2014b; Hou & Zhang, 2015). The Jinshajiang-Ailaoshan suture zone and its surrounding area is the most important Cu-Au metallogenic belt in the Sanjiang region. The Ailaoshan belt in the south is dominated by Au mineralization (e.g.Hu *et al.,* 2004; Hou *et al.,* 2007; Deng *et al.,* 2010; Deng *et al.,* 2011), whereas the Jinshajiang belt in the north is characterized by Cu and Pb-Zn polymetallic mineralization. The Yangla deposit is the largest Cu deposit in the Jinshajiang tectonic belt and contains approximately 150 million tons (Mt) of Cu

ore resources at 1.03% Cu (Fig. 1) (Pan *et al.,* 2001; Zhu *et al.,* 2015).

However, due to the rugged environment, production at the Yangla deposit did not start until 2007. Despite many studies over the past two decades arguing that the Yangla deposit belongs to a intrusion-related Cu skarn system (e.g. Zhu *et al.,* 2015; Meng *et al.,* 2016; Du *et al.,* 2017), the relationship between the granitic magma and the Cu mineralization and ore genesis remain controversial. Some authors argued that the deposit is of a sedimentary exhalative (SEDEX)-type based on fluid inclusion, geochemistry, and C-O isotope studies (Lu *et al.,* 1999, 2004; Pan *et al.,* 2000). Some authors suggested a syngenetic exhalative or volcanogenic genesis as the orebodies show stratigraphic-controlled features (e.g.Lu *et al.,* 1999; Yang *et al.,* 2012), whereas some others suggested the Yangla skarn orebodies formed by SEDEX processes unrelated to intrusive igneous rocks (e.g. Zhan *et al.,* 1998; Zhu et al. 2011). Chen *et al.*
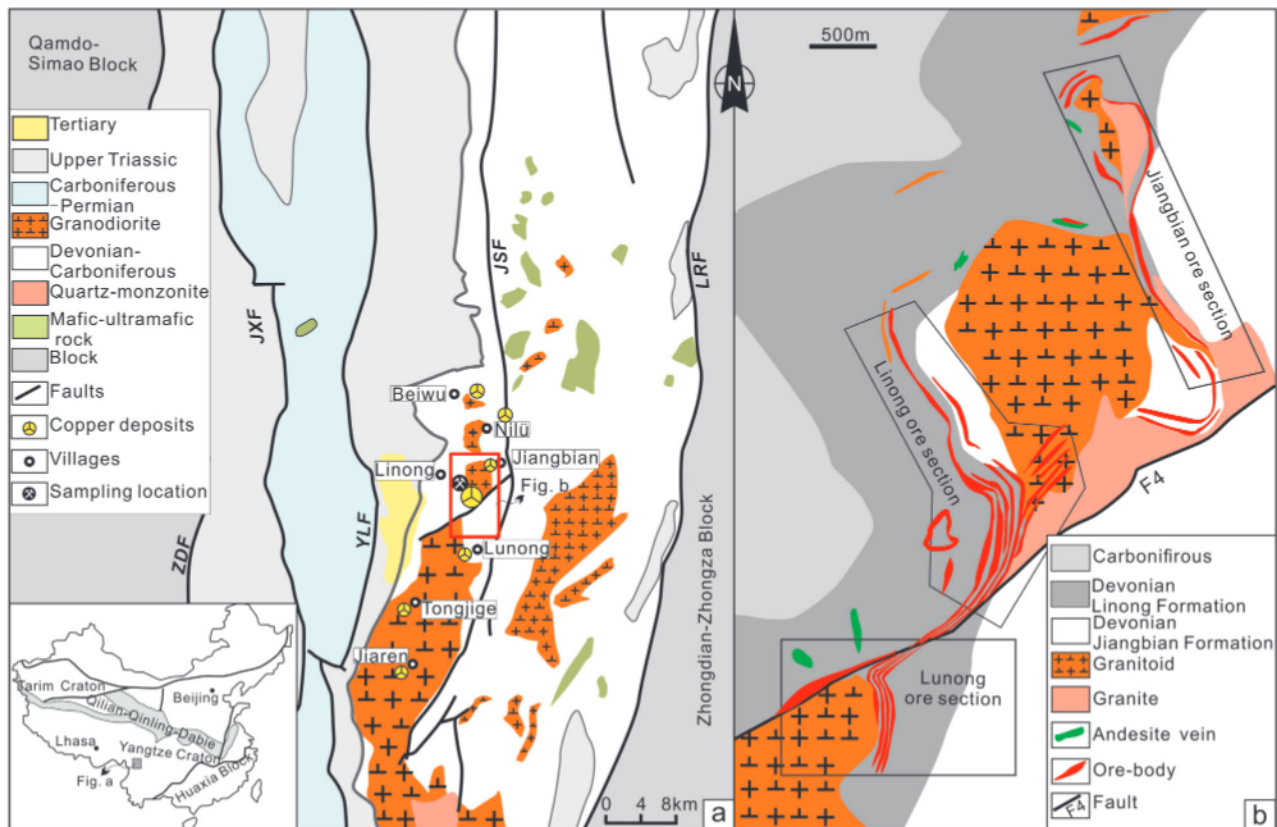

Fig. 1 (a) Geologic map of the Sanjiang region (modified from Zhu, 2012); (b) Geologic map of the Yangla Cu deposit showing the distribution of the major orebodies (modified after Yunnan Copper Group, unpub. data 2004). Abbreviations: JSF, Jinshajiang Fault; JXF, Jiawuxueshan Fault; LRF, Lifu-Riyu Fault; YLF, Yangla Fault; ZDF, Zigasi-Deqen Fault.

(1999) proposed that the Yangla deposit is of a porphyry type, whilst some other authors argued a typical skarn origin associated with granitic intrusions in the area (e.g.Qu *et al.*, 2004; Chen *et al.*, 2013; Zhu *et al.*, 2015; Meng *et al.*, 2016). The long but inconclusive debate is led largely by the lack of systematic and detailed mineralogy and ore-forming mechanisms, as well as the nature and evolution of ore fluid at Yangla.

Fluid inclusions (FIs) trapped in hydrothermal minerals can store important information about the physicochemical conditions of the ore fluids in ancient mineralization systems (Bodnar *et al.*, 2014; Philippot, 2015). Therefore, the nature and evolution of ore fluids are best and most directly demonstrated by FI analyses (e.g. Bodnar *et al.*, 2014; Cao *et al.*, 2015; Lu et al. 2004; Mai & Wang, 1992; Qiu *et al.*, 2015; Robb, 2005; Roedder, 1971; Stefanova *et al.*, 2014; Wilkinson, 2010). Isotope geochemistry is a powerful tool for studying hydrothermal deposits and has been widely applied to constrain the sources of ore fluids and materials. In particular, hydrogen-oxygen (H-O) isotopes have been effectively used to trace the ore fluid origin of hydrothermal deposits (e.g.Hedenquist & Lowenstern, 1994; Zhang *et al.*, 2011; da Costa Silva *et al.*, 2015; Xu *et al.*, 2015; Zhang *et al.*, 2016). Skarn is the most important ore host at Yangla, and quartz is a major gangue mineral, which provides an ideal basis for FI and H-O isotope studies. In this paper, we aim to identify the nature and evolution of fluids in different ore stages and their succession through the analysis of mineralogy, FI, and H-O isotope of altered minerals (e.g. garnet, diopside, and quartz). Published data (Yang, 2012; Zhao, 2012) for Yangla deposits are also compiled with the new data to identify the relationship between the granitic magma and the Cu mineralization of the Yangla deposit.

2.   Ore deposit geology

The Sanjiang region in southwestern China, located in the tectonic junction between Gondwanaland and Eurasia, is the eastern part of the Tethyan-Himalayan tectonic belt (Hou *et al.*, 2003). Several of the Paleozoic sutures in the region record the opening and closure history of the Paleo-Tethys Ocean. Based on the ophiolitic sutures, four main branches for the Paleo-Tethys Ocean have been recognized in this region: the Garzê-Litang Ocean, the Jinshajiang-Ailaoshan Ocean, the Longmu Tso-Shuanghu Ocean, and the Changning-Menglian Ocean (Fig. 1; e.g. Mo *et al.*, 1993; Xiao *et al.*, 2008; Deng *et al.*, 2014b). Numerous igneous rocks and related ore deposits associated with the evolution of each stage of the Paleo-Tethys Ocean were generated (e.g. the Garzê-Litang belt, which includes the Pulang Cu and Gacun Ag polymetallic deposits; the Jinshajiang belt, which includes the Yangla Cu, Yulong Cu (Au-Mo), and Beiya Au (Cu) deposits; e.g. Mo *et al.*, 1993; Hou *et al.*, 2003, 2007; Deng *et al.*, 2014a; Zhu *et al.*, 2015). The Jinshajiang tectonic zone in the eastern Sanjiang region is bounded by the Zhongza-Zhongdian block to the east and by the Qamdo-Simao block to the west (Fig. 1a) (Wang *et al.*, 2000; Pan *et al.*, 2001; Metcalfe, 2013; Wang *et al.*, 2014; Zhu *et al.*, 2015).

The Yangla Cu deposit is located in the middle part of the Jinshajiang tectonic zone and is bounded by the Jinshajiang Fault to the east and the Yangla Fault to the west (Fig. 1a). This deposit consists of seven ore sections (from north to south: Beiwu, Nilü, Jiangbian, Linong, Lunong, Tongjige, and Jiaren), among which the Linong section is the largest and contains ca. 90% of the Yangla Cu reserves (Fig. 1a) (Zhan *et al.*, 1998; Zhu *et al.*, 2015). In this paper, we focus primarily on the Linong section.

2.1   Stratigraphy

The exposed stratigraphy at the Yangla mining district is dominated by Silurian units, the Devonian Jiangbian and Linong Formations, and the Carboniferous Beiwu Formation. The Devonian sequences are the main host for the skarn and orebodies (Fig. 1b). The Silurian sequences consist of quartz schist, biotite-quartz schist, meta-quartz sandstone, and sericite slate and crop out in the southeastern part of the mining district.

The Devonian Jiangbian Formation is located in the middle and southeastern parts of Yangla, and is comprised of three (lower, middle, and upper) members (Figs 1b, 2). The lower member consists of gray meta-quartz sandstone, sericite slate, sericite schist, and fine-grained marble. The middle member mainly consists of light gray sericite-quartz sandstone, sericite slate, sericite-quartz schist, and local occurrences of marble and granitoids. The vein-like orebodies KT6-KT15 are hosted in the interlayer fracture zones in the middle member of the Jiangbian Formation. The upper member is dominated by marble and skarn that are locally interbedded with sericite slate and meta-quartz sandstone, which are the hosts for the orebodies KT4 and KT5.

The Devonian Linong Formation contains hornfels and skarn and is another major skarn ore host at Yangla (Figs 1b, 2). The lower member of the Linong Formation is characterized by interbedded, fine-grained meta-quartz sandstone, sericite slate, marble, and massive garnet/pyroxene skarn, and it hosts the orebodies KT2, KT2-1, KT2-2, and KT3. The middle member of the Linong Formation is dominated by fine- to coarse-grained massive marble, with minor fossils preserved. The upper member consists of inter-bedded, fine-grained, thick-layered to massive marble, sericite slate, meta-quartz sandstone, and minor skarn, and it hosts orebodies KT1 and KT1-1. The Carboniferous Beiwu Formation crops out in the western part of Yangla and consists of sericite slate, marble, and massive basalt.
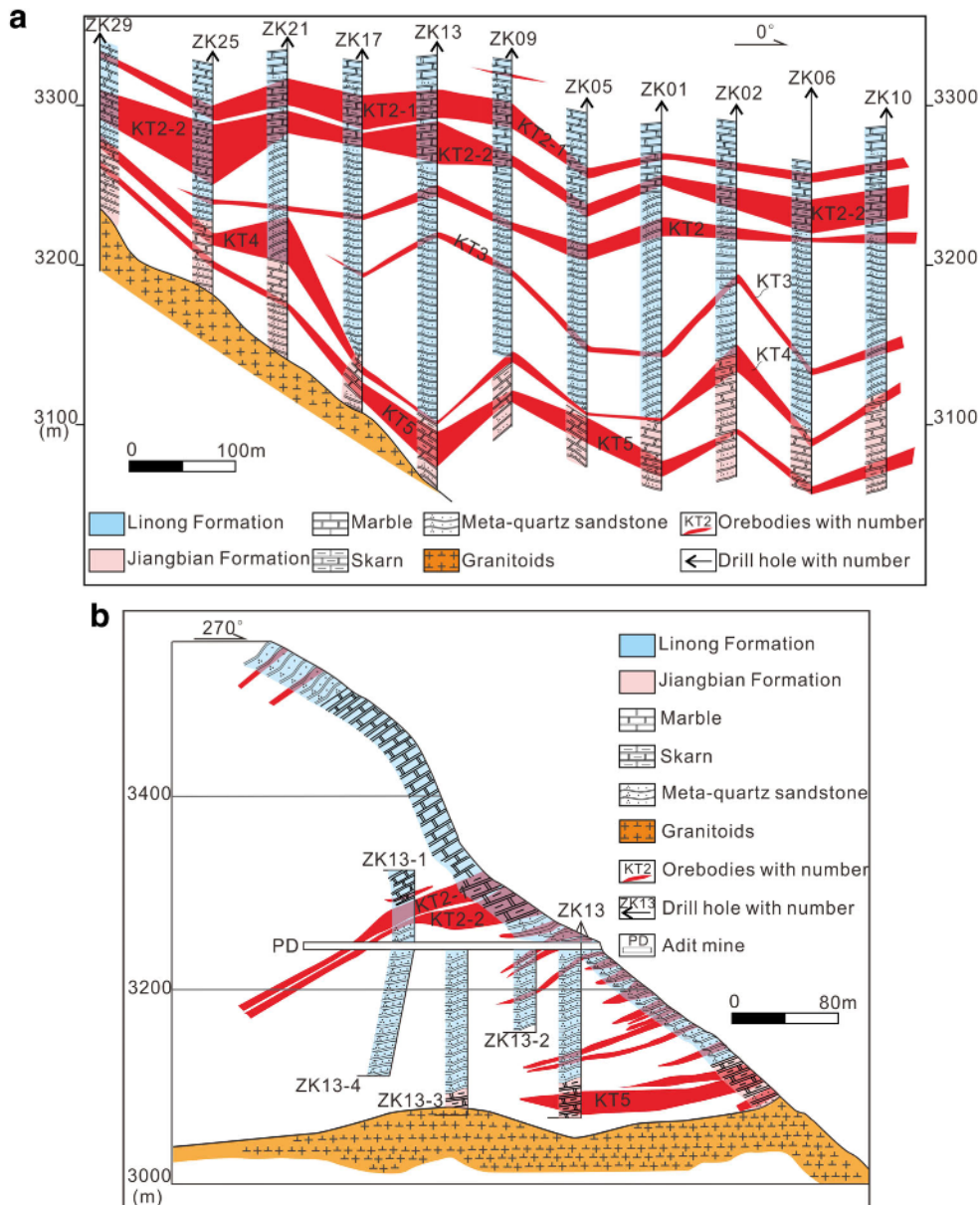

Fig. 2 Geological cross section of the Yangla Cu deposit, showing the spatial relationships between the Devonian stratigraphy, granitoid intrusion, skarn alteration, and Cu mineralization (modified from Yunnan Copper Group, unpub. data 2004).

2.2 Jiaren intrusions

The Jiaren granitoid is the largest granitic intrusion in the Yangla mining district, with an outcrop area of approximately 150 km² (Fig. 1) (Zhu *et al.*, 2015). It intruded the Silurian and Devonian sequences and is composed of granodiorite (dominant), quartz diorite, and biotite quartz monzonite. The granodiorite is medium- to coarse-grained and comprises approximately 40% plagioclase, 15% K-feldspar, 25% quartz, 15% hornblende, and 5% biotite, with accessory zircon, titanite, apatite, and magnetite. The Jiaren granitoid is widely accepted to be I-type with a mixed crustal and mantle origin (Wei *et al.*, 1997; Zhan *et al.*, 1998; Gao *et al.*, 2010; Zhu *et al.*, 2011b). Zhu *et al.* (2011a) concluded that these I-type granitoids are enriched in abundances of Si and large ion lithophile elements but are depleted in high field strength elements and might contain relatively high water concentrations and high magmatic oxidation state. It was emplaced in the early Late Triassic (SIMS zircon U–Pb dating: 233 ± 1.4and 231.0 ± 1.6 Ma; Zhu *et al.*, 2011a, 2015) and is coeval with the Yangla Cu mineralization (molybdenite Re-Os dating: ca. 232 Ma; Yang *et al.*, 2012; Zhu *et al.*, 2015). This suggests a possible genetic link between the Jiaren granitoid and Cu mineralization.

2.3 Structure

The Yangla deposit is N–S-trending (elongated) and is bounded by the Jinshajiang Fault to the east and the Yangla Fault to the west (Fig. 1a; Zhan *et al.*, 1998). The Jinshajiang Fault is a regional-scale thrust that dips 60–80° to the west, and the Yangla Fault dips 30–70° to the east (Zhu *et al.*, 2015). The north-east-trending normal fault F4 in the middle part of Yangla (approximately 6 km long) has dip angles of 42–80° (Fig. 1b) (Yunnan Copper Group 2004 unpub.). In addition, interlayer fracture zones are widely developed by regional compression during the Triassic Indosinian Orogeny and by the Jiaren granitoid emplacement (Zhan *et al.*, 1998). The Linong anticline and the Jiangbian syncline are the major fold structures in the mining district (Yunnan Copper Group 2004 unpub.).

2.4 Alteration and mineralization

Wall rock alterations are widespread at Yangla and consist mainly of skarn, silicic, and carbonate (Fig. 3). The skarn alteration is mainly exoskarn around the granitoid intrusions in the intruded Devonian carbonate rocks (Figs 2–3). The prograde (anhydrous) skarn
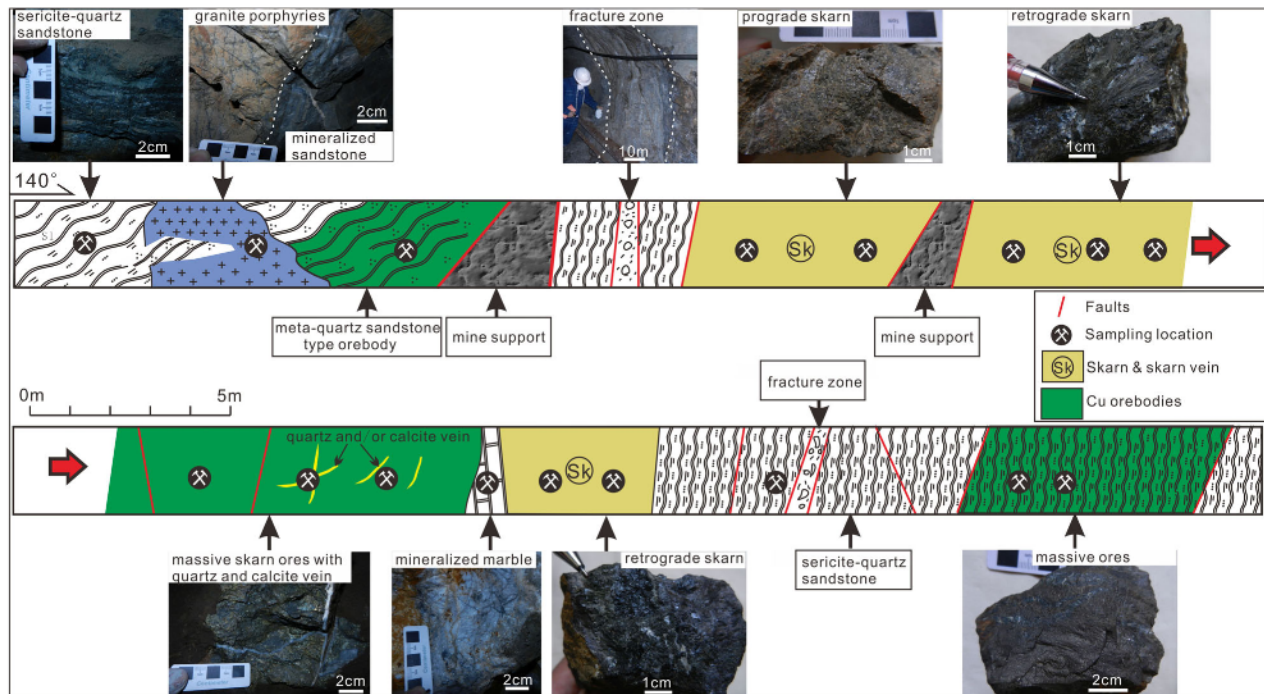

Fig. 3 A sketch map of the 3250-m section of tunnel in stope 41# for the Yangla Cu deposit, showing that Cu orebodies are closely associated with skarn alteration within the Devonian carbonate rocks.

assemblage is characterized by reddish-brown to sage green, coarse-grained garnet and gray to dark green pyroxene (Fig. 4c, g). Individual garnet crystals are typically 0.1–0.5 cm in diameter and lack obvious compositional zoning, whereas the pyroxene crystals are generally smaller (Fig. 4c). The retrograde (hydrous) alteration assemblage is dominated by epidote, chlorite, and sericite, which locally replaces the prograde skarn minerals (Figs 3–4c, 5d, e). Magnetite, pyrite, pyrrhotite, and chalcopyrite generally coexist
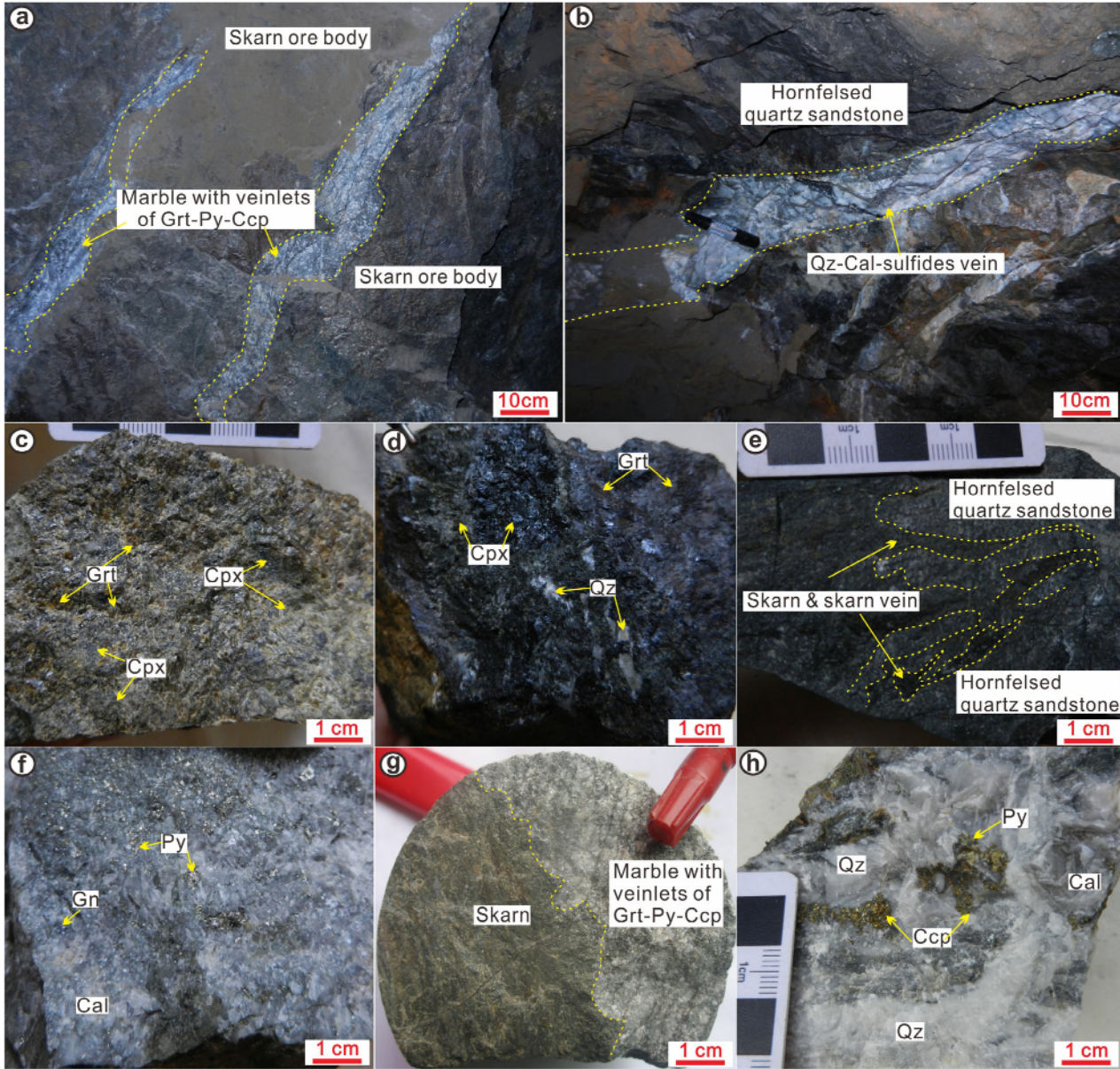
Fig. 4 Photographs of the Yangla Cu deposit. (a) Marble vein in a skarn orebody; (b) quartz-calcite-sulfide vein along an interlayer fracture zone in a hornfels quartz sandstone; (c) reddish-brown coarse-grained garnet coexisting with clinopyroxene in skarn; (d) dark-green clinopyroxene coexisting with fine-grained garnet and quartz skarn; (e) skarn veins in a hornfels quartz sandstone; (f) marble with euhedral pyrite and galena; (g) skarn contacts with bleached white marble and garnet-sulfide veinlets; (h) disseminated sulfides in a stage IIb quartz-calcite vein. Abbreviations: Cal, calcite; Ccp, chalcopyrite; Cpx, clinopyroxene; Gn, galena; Grt, garnet; Py, pyrite; Qz = quartz.

with the retrograde alteration minerals, forming densely disseminated or massive skarn ores (Fig. 3). The quartz sandstone is generally hornfels with skarn vein intrusion (Fig. 4e). The skarn commonly displays metasomatic contact with the marble, in which garnet sulfide veinlets are widespread (Figs 3–4g). The silicic and carbonate (calcite) alterations commonly overprint the earlier skarn (Fig. 4d; Fig. 5b, d, e).

Spatially, the Yangla Cu mineralization is closely associated with retrograde skarn alteration (Fig. 3).

The orebodies are generally stratiform/lenticular in the exoskarn zones or within the intrusion–distal interlayer fracture zones (Fig. 1b; Fig. 2). The Linong ore section contains 20 orebodies. The major orebodies KT2-1, KT2-1, KT4, and KT5 are mainly skarn ores and account for 90% of the Cu resources in this ore section. Individual orebody ranges are as follows: <1–44 m thick, 1140–2200 m long, and generally dip gently (8–22°) to the northwest (except for KT2-1 and KT2-2, which dip steeply from 30° to 40° at
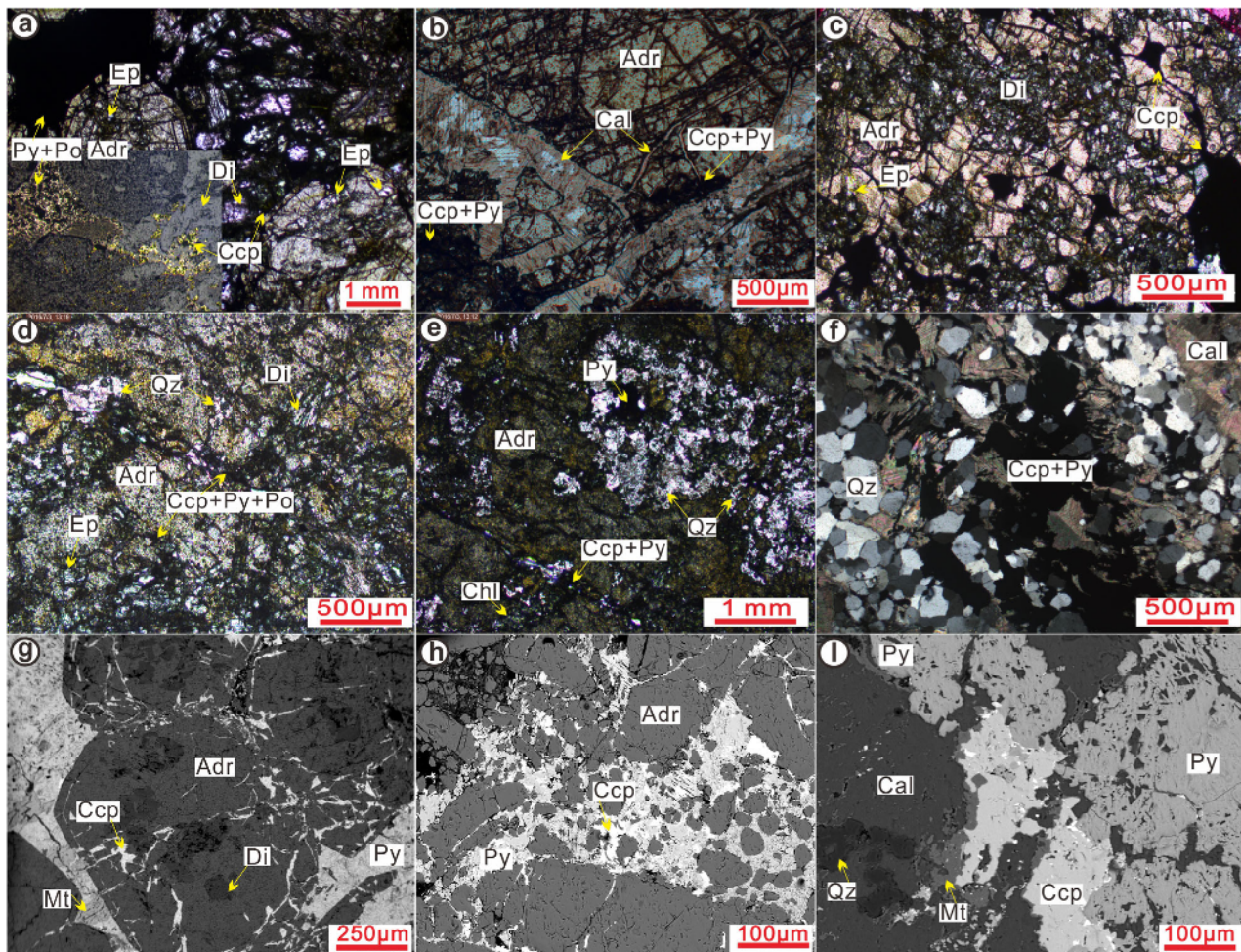

Fig. 5 Representative photomicrographs showing mineral assemblages and textural features of the Yangla Cu deposit. (a) Adr coexisting with Di and interstitial Fe-Cu sulfides between Adr and Di (PPL, RFL in lower-left corner); (b) calcite and sulfides between Adr or replacing Adr in skarn ores (PPL); (c) Adr coexisting with Di and interstitial Ccp between Adr (PPL); (d) and (e) Adr replaced by fine-grained Ep, Chl, and Qz, plus interstitial Cu-Fe sulfides (PPL); (f) and (i) Fe-Cu sulfides in quartz-calcite vein from the late ore sub-stage (CPL in f, BSE in i); (g) and (h) Fe-Cu sulfides crosscutting or interstitial between Adr (BSE). Abbreviations: BSE, backscattered electron images; CPL, crossed polarized light; PPL, plane polarized light; RFL, reflect light. Adr, andradite; Cal, calcite; Ccp, chalcopyrite; Chl, chlorite; Di, diopside; Ep, epidote; Po, pyrrhotite; Py, pyrite; Qz, quartz.

depth) (Fig. 2). These orebodies typically show metasomatic contact with the marble (Fig. 4a, g). Copper sulfides (e.g. bornite and chalcopyrite) commonly occur as fine- to coarse grains and coexist with pyrrhotite, pyrite, galena, and sphalerite, forming the disseminated or massive skarn ores.

2.5 Paragenesis

Three alteration/mineralization stages (i.e. pre-ore, syn-ore, and supergene) have been identified in the Yangla deposit (Fig. 6). The pre-ore stage (I) is mainly marked by the presence of anhydrous prograde skarn minerals, such as garnet (andradite/grossular) and clinopyroxene (diopside/hedenbergite), and the lack of sulfides (Fig. 4c, d; Fig. 5c, h). The syn-ore stage (II) is characterized by the presence of hydrous silicate minerals, quartz, calcite, and abundant metallic minerals, including Fe oxides and Cu-Mo-Fe sulfides. Based on petrographic crosscutting relationships and mineral paragenesis, the syn-ore stage can be divided into two substages (Fig. 6). The early syn-ore stage (IIa) contains retrograde alteration minerals, including hydrous silicates (e.g. actinolite, epidote and chlorite), Fe oxides, and abundant Cu-Mo-Fe sulfides; quartz; and minor calcite. Magnetite, pyrite, chalcopyrite, pyrrhotite, and molybdenite occur as disseminated fine-grained

anhedral crystals that coexist with quartz and calcite or as massive ores in the marble and skarn (Fig. 4d; Fig. 5a–e, g–h). The late syn-ore stage (IIb) is associated with silicic and carbonate alterations and is represented by widespread thick quartz/calcite veins. The late syn-ore stage pyrite, chalcopyrite, galena, and sphalerite occur as coarse-grained, subhedral to euhedral crystals in the quartz/calcite veins (Fig. 4b, h; Fig. 5f, i). The supergene stage (III) is dominated by secondary Cu minerals, including azurite and malachite, which replaced primary chalcopyrite and bornite.

3. Samples and analytical methods

All of the unweathered samples in this study were collected from underground mining tunnels in the Linong ore section (Fig. 3). To identify the mineral assemblages and paragenetic sequence, thin sections of all the samples were examined under an optical microscope.

Mineral chemical analyses were performed at the State Key Laboratory of Ore Deposit Geochemistry of the Institute of Geochemistry Chinese Academy of Sciences using an EPMA-1600 Electron Probe Micro Analyzer (EPMA) operated with an accelerating voltage of 25 kV, a beam current of 10 nA, and a beam

Minerals	Pre-ore stage (I)	Syn-ore stage (II)		Supergene stage (III)
		Early syn-ore stage (IIa)	Late syn-ore stage (IIb)	
Garnet (Adr)	▬▬▬			
Diopside	▬▬▬			
Hedenbergite	▬▬			
Epidote		▬▬▬		
Actinolite		▬▬▬		
Magnetite		▬▬		
Sericite		▬▬▬		
Chlorite		▬▬▬▬		
Pyrrhotite		▬▬▬		
Molybdenite		▬▬▬		
Pyrite		▬▬▬▬▬▬	▬▬▬▬	
Chalcopyrite		▬▬▬▬▬▬	▬▬▬▬	
Quartz		▬▬▬▬	▬	
Calcite		▬▬	▬▬▬	
Galena			▬▬▬	
Sphalerite			▬▬▬	
Malachite				▬▬▬
Azurite				▬▬▬

Fig. 6 Mineral paragenesis of the Yangla Cu deposit.

size of 10 μm. Minimum detection limits for all the analyzed elements are around 200 ppm.

Fluid inclusions (FIs) were examined in garnet, clinopyroxene, and quartz (quartz-IIa) from the skarn ores (Fig. 4d; Fig. 5d, e) and in the quartz (quartz-IIb) and calcite from the quartz-calcite-sulfide veins (Fig. 4b, h; Fig. 5f). The FIs in the quartz and calcite were measured using a Linkam THMSG600 programmable freezing–heating stage mounted on a Leica microscope. Because the relatively dark colors of garnet and clinopyroxene make potential FIs difficult to observe, microthermometric measurements of the FIs in garnet and clinopyroxene were performed on a heating–freezing system mounted on an Olympus BH51 infrared microscope. Moritz (2006) suggested that the temperatures of phase changes measured using infrared microthermometry on opaque minerals should be interpreted with care because the temperatures can vary with the intensity of the infrared light source, which may result in underestimations of homogenization temperatures and overestimations of fluid salinities. To minimize these effects, the microthermometric analyses were conducted carefully with the lowest possible light intensity and with all of the possible diaphragms nearly closed (Moritz, 2006). The uncertainty of the temperature measurements in this study was approximately ±0.2°C below 50°C and ±2°C at higher temperatures. All the samples were initially cooled to −100°C before being slowly warmed to measure the first ice melting and final melting temperatures. The heating/cooling rates were restricted to <15°C/min and 1–0.1°C/min near the phase transformations. The vapor compositions of individual FIs in garnet, clinopyroxene, and quartz were identified using laser Raman spectroscopy.

The salinities of the two-phase aqueous inclusions were calculated using the final melting temperatures of the ice following the methods proposed by Bodnar (1993) and Lu et al. (2004). Bulk composition and density of the aqueous and carbonic phases of the two-phase aqueous inclusions were calculated using an online calculator (gcmodel.kl-edi.ac.cn/archives/).

Gangue minerals of garnet (pre-ore stage), quartz-IIa (early syn-ore stage; Figs 4d, 5d, e), and quartz-IIb (late syn-ore stage; Figs 4b, h, 5f) were selected from the Cu ores to analyze the mineral oxygen isotopes and FI hydrogen isotopes. The Cu ore samples were crushed to 40–80 mesh, and mineral grains were then handpicked under a binocular microscope. Single-mineral samples were crushed to 200 mesh using an agate mill, and the oxygen isotope analyses were

performed using the BrF_5 method to obtain CO_2 (Clayton & Mayeda, 1963). Procedures for the hydrogen isotope analysis required water to be released from the FIs after heating. Therefore, the single-mineral samples were crushed to 40–60 mesh and put into a quartz tube for heating. The released water was then reacted with heated CuO and zinc to produce hydrogen, which was transferred to an activated carbon sample collection quartz tube surrounded by liquid nitrogen (Coleman *et al.*, 1982). The $\delta^{18}O$ and δD values were measured using a Thermo MAT-253 stable isotope ratio mass spectrometer at the Geological Analysis Laboratory of the Ministry of Nuclear Industry (Beijing, China). The analytical precisions were ±0.2‰ for oxygen and ±2‰ for hydrogen. The O-H isotope compositions are expressed in per mil relative to Vienna Standard Mean Ocean Water (V-SMOW). The garnet–water and quartz–water fractionation equations of Zheng (1993) were used to calculate the $\delta^{18}O$ values of the fluids in equilibrium with the silicate minerals.

4. Results

4.1 Mineralogy and chemical compositions

Based on the observations of skarn hand specimens and thin sections (Figs 4c, d, 5a-e, g-h), the prograde skarn consists mainly of garnet and minor clinopyroxene. Representative EPMA data from the garnet and clinopyroxene are given in Table 1 and plotted in Figure 7. The garnet is commonly fine- to coarse-grained and euhedral to subhedral. All the green and yellowish/reddish-brown garnets are highly andraditic, with an average Adr% value of 90 (Table 1; Fig. 7). The garnets have distinct colors but rarely display clear oscillatory zoning (Fig. 5a-c, g-h) and generally have similar major element chemistry, which suggest no correlation between the colors and the major element compositions. The highly andraditic compositions of the garnets indicate that the pre-ore stage (I) hydrothermal fluid was likely oxidized and Fe-rich (Maher, 2010). The clinopyroxene intergrown with the garnet is generally pale to dark green and comprises mainly diopside with a mean Di% value of 86 (Table 1; Fig. 7). The Mn/Fe ratios of the clinopyroxene range mainly between 0.03 and 0.11 (mean 0.07). Compositionally, the Yangla garnet and clinopyroxene have major element contents consistent with those from Cu skarn

Table 1 Representative EPMA data of garnet and clinopyroxene (wt %) from the Yangla Cu deposit

Sample No.	Grt-1	Grt-2	Grt-3	Grt-4	Grt-5	Grt-6	Grt-7	Grt-8	Grt-9	Grt-10	Cpy-1	Cpy-2	Cpy-3	Cpy-4	Cpy-5	Cpy-6	Cpy-7	Cpy-8	Cpy-9	Cpy-10
SiO_2	35.44	35.73	35.59	34.68	36.55	36.02	35.83	36.31	36.09	35.69	54.36	50.37	53.28	53.85	53.73	53.86	51.62	54.38	53.46	54.94
TiO_2	0.02	0.03	0.13	0.00	0.00	0.01	0.00	0.00	0.01	0.01	0.02	0.02	0.02	0.01	0.00	0.01	0.00	0.02	0.02	0.01
Al_2O_3	0.51	0.03	0.47	0.76	0.00	0.00	0.01	0.02	0.00	0.01	0.33	2.07	0.48	0.58	0.46	0.62	0.16	0.38	0.60	0.15
Cr_2O_3	0.01	0.02	0.00	0.00	0.00	0.02	0.04	0.00	0.02	0.17	0.00	0.05	0.03	0.00	0.01	0.00	0.00	0.00	0.00	0.00
FeO	28.75	29.00	27.55	28.33	29.46	28.59	29.10	29.17	29.13	28.55	3.50	11.28	3.81	3.82	3.75	4.72	13.00	2.40	3.83	1.92
MnO	0.20	0.22	0.18	0.27	0.13	0.18	0.15	0.14	0.21	0.16	0.24	0.30	0.27	0.21	0.22	0.30	0.78	0.56	0.27	0.46
MgO	0.08	0.00	0.16	0.03	0.05	0.09	0.08	0.04	0.07	0.12	15.89	13.99	15.56	15.51	15.01	13.92	9.17	15.26	14.93	16.43
CaO	34.18	34.03	33.74	33.88	34.64	34.37	34.51	34.52	34.40	34.45	26.20	18.78	26.31	26.31	26.22	25.82	24.75	26.77	25.98	26.47
Na_2O	0.00	0.00	0.02	0.03	0.00	0.01	0.00	0.00	0.00	0.37	0.02	0.01	0.02	0.00	0.00	0.03	0.06	0.06	0.04	0.14
K_2O	0.00	0.00	0.00	0.00	0.00	0.00	0.00	0.00	0.00	0.03	0.00	0.02	0.00	0.00	0.00	0.01	0.00	0.00	0.01	0.01
total	99.19	99.05	97.84	97.97	100.82	99.29	99.72	100.21	99.92	99.54	100.55	96.86	99.78	100.30	99.38	99.29	99.53	99.83	99.14	100.53
Si	2.94	2.96	2.98	2.92	2.98	2.98	2.96	2.98	2.97	2.96	1.99	1.95	1.97	1.98	1.99	2.00	1.99	2.00	1.99	2.00
Ti	0.00	0.00	0.01	0.00	0.00	0.00	0.00	0.00	0.00	0.00	0.00	0.00	0.00	0.00	0.00	0.00	0.00	0.00	0.00	0.00
Al	0.05	0.00	0.05	0.08	0.00	0.00	0.00	0.00	0.00	0.00	0.00	0.09	0.00	0.03	0.02	0.03	0.01	0.02	0.03	0.01
Cr	0.00	0.00	0.00	0.00	0.00	0.00	0.00	0.00	0.00	0.01	0.00	0.00	0.00	0.00	0.00	0.00	0.00	0.00	0.00	0.00
Fe^{3+}	1.99	2.01	1.93	1.98	2.01	1.98	2.01	2.00	2.00	1.98	0.02	0.01	0.06	0.03	0.00	0.00	0.01	0.00	0.01	0.02
Fe^{2+}	0.00	0.00	0.00	0.01	0.00	0.00	0.00	0.00	0.00	0.00	0.09	0.35	0.06	0.09	0.11	0.15	0.41	0.07	0.11	0.04
Mn	0.01	0.02	0.01	0.02	0.01	0.01	0.01	0.01	0.01	0.01	0.01	0.01	0.01	0.01	0.01	0.01	0.03	0.02	0.01	0.01
Mg	0.01	0.00	0.02	0.00	0.01	0.01	0.01	0.01	0.01	0.01	0.87	0.81	0.86	0.85	0.83	0.77	0.53	0.84	0.83	0.89
Ca	3.04	3.03	3.03	3.05	3.02	3.05	3.05	3.03	3.03	3.06	1.03	0.78	1.04	1.03	1.04	1.03	1.02	1.05	1.03	1.03
Na	0.00	0.00	0.00	0.00	0.00	0.00	0.00	0.00	0.00	0.01	0.01	0.00	0.00	0.00	0.00	0.00	0.00	0.00	0.00	0.01
K	0.00	0.00	0.00	0.00	0.00	0.00	0.00	0.00	0.00	0.00	0.00	0.00	0.00	0.00	0.00	0.00	0.00	0.00	0.00	0.00
Adr / Di	97.54	99.24	94.60	96.35	99.08	96.66	98.10	98.44	98.43	96.24	90.32	69.10	92.77	90.15	87.27	83.13	55.00	90.19	87.45	94.14
Grs / Hed	1.58	0.19	4.35	2.59	0.43	2.50	1.14	1.06	0.78	2.41	8.91	30.07	6.31	9.15	12.00	15.86	42.34	7.95	11.64	4.38
Pyr / Jo	0.88	0.57	1.05	1.06	0.49	0.84	0.76	0.50	0.79	1.35	0.76	0.83	0.92	0.70	0.72	1.01	2.65	1.87	0.91	1.48

Adr, andradite; Di, diopside; Grs, grossular; Hed, hedenbergite; Jo, johannsenite; Pyr, pyralspite (pyrope + almandine + spessartine).
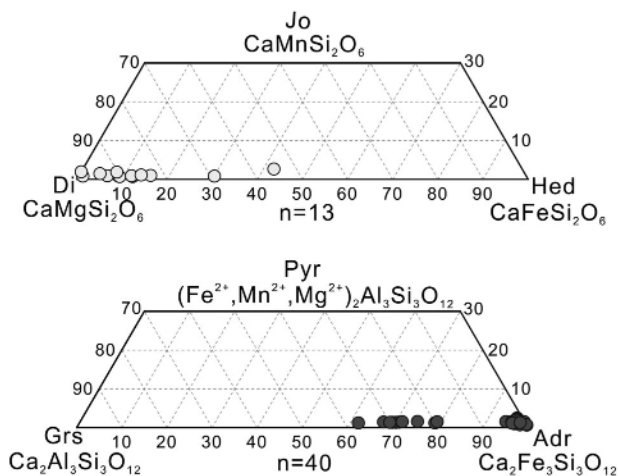
Fig. 7 Ternary diagrams showing garnet and clinopyroxene compositions in the Yangla skarn. Abbreviations: Adr, andradite; Di, diopside; Grs, grossular; Hed, hedenbergite; Jo, johannsenite; Pyr, pyralspite (pyrope + almandine + spessartine).

deposits around the world (Nakano *et al.*, 1994; Meinert *et al.*, 1997; Meinert *et al.*, 2005).

4.2 Fluid inclusions

4.2.1 FI types and occurrence

Three types of primary FIs were recognized at Yangla based on the nature of the phase relationships at room temperature and the phase transitions during cooling and heating: two-phase liquid-rich (L-type), two-phase vapor-rich (V-type), and halite-bearing (S-type) FIs.

The L-type FIs consist of a liquid phase and a 5–30 vol.% vapor phase. These inclusions are commonly irregular or negative crystal in shape, 3–15 μm in size, and occur in clusters or as individual inclusions in garnet, clinopyroxene, quartz, and calcite (Fig. 8c-d, f-i).

The V-type FIs are typically characterized by a dark vapor bubble that occupies over 50 vol%. They are largely 3–13 μm in size and have an elliptical or negative crystal shape. The V-type inclusions commonly occur in clusters with S-type or L-type FIs in garnet, clinopyroxene, and quartz-IIa (Fig. 8a, c, f-g).

The S-type FIs contain a vapor bubble, a liquid phase, and a cubic halite daughter mineral. These inclusions generally occur as negative crystals and are

8–24 μm in size. These FIs are commonly found in garnet and clinopyroxene (Fig. 8a-b, e).

In summary, the stage I garnet and clinopyroxene contain more abundant V-type, S-type, and L-type FIs. The quartz-IIa contains more L-type and V-type FIs (Fig. 8g-h), whereas L-type FIs are more common in stage IIb quartz-IIb and calcite (Fig. 8i).

4.2.2 Microthermometric results

Microthermometric results for the Yangla FIs are listed in Table 2 and illustrated in Figure 9. According to the criteria proposed by Lu et al. (2004) and Roedder (1984), only the primary FIs were interpreted. Although V-type inclusions occur with S-type and/or L-type inclusions in garnet, clinopyroxene, and quartz-IIa, measurement of their ice-melting temperatures are difficult due to the poor visibility and their small size. The L-type and S-type inclusions were homogenized to liquids during heating, and the halite in the S-type inclusions dissolved before the vapor bubble disappeared. It is noteworthy that several L-type, S-type, and V-type inclusions in garnet did not homogenize at temperatures below 500°C (upper temperature limit of the microthermometric stage), which resulted in the average homogenization temperatures of FIs in garnet being lower than the reality.

V-type inclusions typically coexist with S-type or L-type inclusions in garnet, clinopyroxene, and quartz-IIa (Fig. 8a, c, f-g). These FIs homogenized at 458–499°C (average 479°C, n = 4) in garnet, 378–493°C (average 452°C, n = 5) in clinopyroxene, and 375–403°C (average 391°C, n = 4) in quartz-IIa.

S-type FIs are commonly present in stage I garnet and clinopyroxene, and those in garnet homogenized at 499°C (n = 1; several other FIs did not homogenize below 500°C). The halite dissolution temperatures vary from 397 to 493°C, which correspond to salinities of 46.4–58.4 wt.% NaCl eqv. (average 51.5 wt.% NaCl eqv., n = 3). The S-type inclusions in clinopyroxene homogenized at 379–481°C (average 439°C, n = 4), with their halite dissolution temperatures being 274–341°C, which correspond to salinities of 36.0–41.5 wt.% NaCl eqv. (average 39.5 wt.% NaCl eqv., n = 5). The densities of these inclusions in the garnet and clinopyroxene are 1.345–1.345 g/cm^3 and 1.084–1.088 g/cm^3, respectively.

L-type inclusions in the stage I garnet and clinopyroxene yielded ice-melting temperatures of −21.1 to −9.0°C and −20.8 to −15.7°C, respectively, with
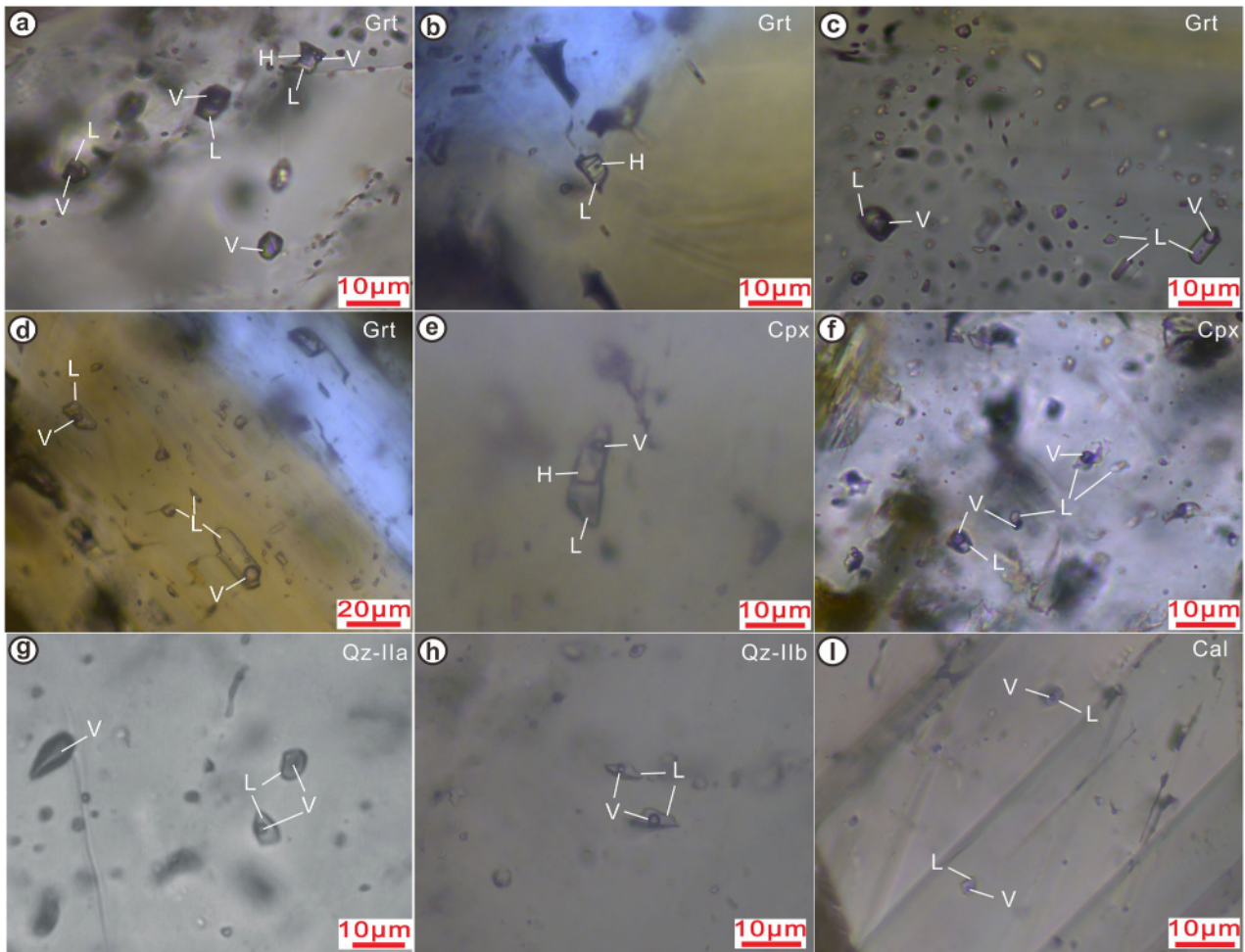
Fig. 8 Microphotographs showing different types of fluid inclusions (FIs) from Yangla. **(a)** S-type, V-type, and L-type FIs coexist in stage I garnet, showing evidence of fluid boiling; **(b)** and **(e)** S-type FIs in garnet and clinopyroxene; **(c)** and **(f)** V-type and L-type FIs coexist in garnet and clinopyroxene, implying fluid boiling in the pre-ore stage; **(d)** L-type FIs in garnet; **(g)** V-type and L-type FIs coexist in quartz-IIa, implying fluid boiling in the early ore substage; **(h)** and **(i)** L-type FIs in stage IIb quartz and calcite. Abbreviations: Cal, calcite; Ccp, chalcopyrite; Cpx, clinopyroxene; Grt, garnet; L-type, two-phase liquid-rich; Qz-IIa and Qz-IIb, quartz from early and late ore substages, respectively; S-type, halite-bearing; V-type, two-phase vapor-rich.

corresponding salinities of 12.9–23.1 wt.% NaCl eqv. (average 18.3 wt.% NaCl eqv., n = 16) and 19.2–22.9 wt.% NaCl eqv. (average 21.1 wt.% NaCl eqv., n = 6), respectively. The homogenization temperatures vary from 372 to 499°C (some >500°C) (average = 453°C, n = 18) for the inclusions in garnet and from 366 to 492°C (average 431°C, n = 16) for those in clinopyroxene. The densities of these inclusions vary from 0.494 to 0.817 g/cm^3 and from 0.692 to 0.821 g/cm^3, respectively.

The homogenization temperatures of the L-type FIs in quartz-IIa vary from 301 to 415°C (average 351°C,

n = 21). The ice-melting temperatures of these inclusions range from −8.0 to −1.6°C, corresponding to salinities of 2.6–11.7 wt.% NaCl eqv. (average 7.5 wt.% NaCl eqv., n = 13). Their densities are between 0.576 and 0.829 g/cm^3.

L-type FIs are widespread in the quartz-IIb and calcite from the late ore substage and have homogenization temperatures that range from 165 to 294°C (average 238°C, n = 31) and from 142 to 283°C (average 185°C, n = 18), respectively. The ice-melting temperatures of these inclusions in quartz-IIb and calcite are between −5.2 and −1.0°C and between −2.9 and

Table 2 Microthermometric data on fluid inclusions (FIs) in the Yangla Cu deposit

Host mineral	FI type	Th (°C)		Tm, ice (°C)		Tm (°C)		Salinity (wt % NaCl equiv.)		Density (g/cm³)	
		Range (n)	Ave	Range (n)	Ave	Range (n)	Ave	Range (n)	Ave	Range (n)	Ave
Pre-ore stage											
Andradite	L	372 to 499 (18)	453	−21.1 to −9.0 (16)	−14.9			12.9 to 23.1	18.3	0.494 to 0.817	0.671
	V	458 to 499 (4)	479								
	S	499 to 499 (1)	499			397.1 to 492.7 (3)	437.8	46.4 to 58.4	51.5	1.345 to 1.345	1.345
Diopside	L	366 to 492 (16)	431	−20.8 to −15.7 (6)	−18.3			19.2 to 22.9	21.1	0.692 to 0.821	0.744
	V	378 to 493 (5)	452								
	S	379 to 481 (4)	439			273.5 to 341.2 (5)	319	36.0 to 41.5	39.5	1.084 to 1.088	1.085
Early ore substage											
Quartz-IIa	L	301 to 415 (21)	351	−8.0 to −1.6 (13)	−4.8			2.6 to 11.7	7.5	0.576 to 0.829	0.730
	V	375 to 403 (4)	391	−2.5 to −1.8 (3)	−2.1			3.1 to 4.2	3.5	0.486 to 0.563	0.530
Late ore substage											
Quartz-IIb	L	165 to 294 (31)	238	−5.2 to −1.0 (26)	−2.6			1.7 to 8.1	4.4	0.755 to 0.943	0.851
Calcite	L	142 to 283 (18)	185	−2.9 to −0.8 (15)	−1.6			1.4 to 4.8	2.7	0.754 to 0.947	0.894

L, liquid-rich; V, vapor-rich; S, daughter mineral-bearing; Th (°C), final homogenization temperature; Tm, ice (°C), temperature of ice point; Tm (°C), dissolution temperature of halite; Ave, average; (n), number of measurements. Seven L-type inclusions, two S-type inclusions in andradite, and one L-type inclusion in diopside with Th > 500 °C were not included in the table. No Tm or ice data were measured from the V-type inclusions.

−0.8°C, respectively, which correspond to salinities of 1.7–8.1 wt.% NaCl eqv. (average 4.4 wt.% NaCl eqv., n = 26) and 1.4–4.8 wt.% NaCl eqv. (average = 2.7 wt.% NaCl eqv., n = 15), respectively. The densities of these inclusions in quartz-IIb and calcite vary from 0.755 to 0.943 g/cm³ and from 0.754 to 0.947 g/cm³, respectively.

V-type FIs typically coexist with S-type or L-type inclusions (Fig. 8a, c, f-g). These two FI types have similar homogenization temperatures, which is clear evidence of fluid boiling.

4.2.3 *Pressure estimation and mineralization depth*

Estimates of trapping pressure can be obtained only when the actual fluid entrapment temperature is known or if fluid boiling or immiscibility occurred at the time of FI entrapment (Roedder and Bodnar 1980; Roedder, 1984). Pressures determined for non-boiling assemblages can be derived from the homogenization temperature and represent the minimum values (Rusk *et al.*, 2008). As described above, fluid-boiling FI assemblages at Yangla were found inside garnet, clinopyroxene, and quartz-IIa as evidenced by the close spatial relationship between the V-type and the L- and S-type FIs (Fig. 8a, c, f-g) and the similar homogenization temperatures and contrasting

salinities of these inclusions. Thus, the homogenization temperatures are interpreted to closely approximate the trapping temperatures and the trapping pressures can be estimated using the isobar equations from Driesner and Heinrich (2007). However, the lack of evidence for boiling in stage IIb quartz and calcite only permits the minimum trapping P–T estimation. Based on the total homogenization temperatures and salinities of the L-, V-, and S-type FIs, the trapping pressures of the FIs can be approximated in the binary NaCl-H_2O system (Hedenquist *et al.*, 1998; Driesner & Heinrich, 2007).

As shown in Figure 10, the trapping pressures of the FIs in the stage I garnet and clinopyroxene, quartz-IIa, and stage IIb quartz and calcite cluster around 400–600 bars, 100–300 bars, and 10–50 bars, respectively. These pressures are equivalent to a trapping depth of approximately 2 km if lithostatic pressure is assumed in the high-temperature pre-ore stage and hydrostatic pressure is assumed in the lower-temperature syn-ore stage.

4.2.4 *Laser Raman spectroscopy analysis*

Laser Raman microspectroscopic analysis of representative inclusions shows that the vapor phase in the L-type FIs in the garnet and clinopyroxene consists
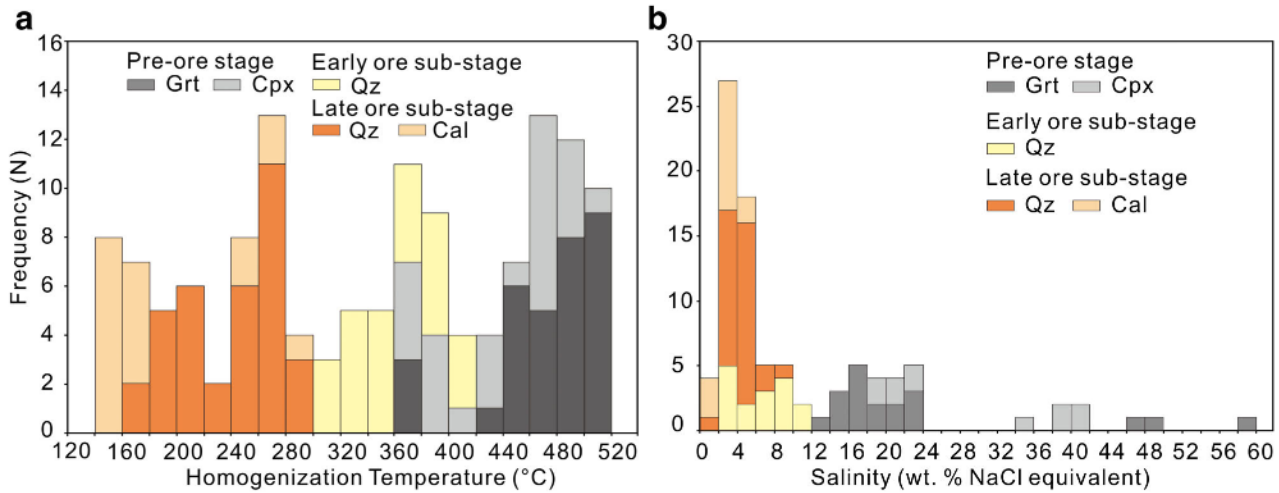
Fig. 9 Histograms of homogenization temperatures (a) and salinities (b) for all inclusion types of the different alteration/mineralization stages. Abbreviations: Cal, calcite; Cpx, clinopyroxene; Grt, garnet; Qz, quartz.
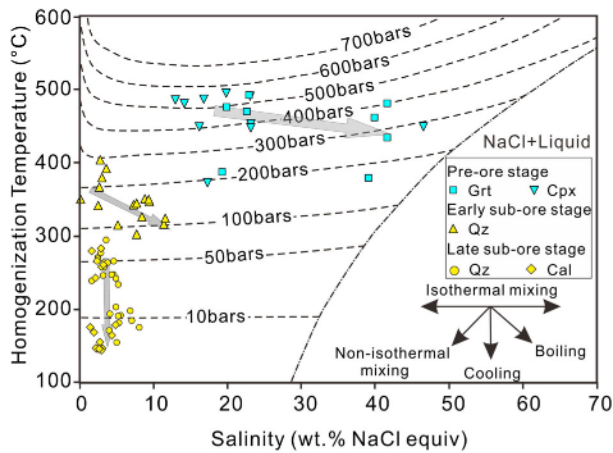

Fig. 10 Pressure estimations for all inclusion types of the different alteration/mineralization stages at Yangla. The arrows show the interpreted trends of the fluids. I, II, III, and IV represent isothermal mixing, non-isothermal mixing, cooling, and boiling, respectively. Abbreviations: Cal, calcite; Cpx, clinopyroxene, Grt, garnet; Qz, quartz.

primarily of H_2O (Fig. 11a-b), whereas that in the L-type FIs in the quartz-IIa/-IIb is dominated by H_2O with minor CH_4, N_2, and CO_2 (Fig. 11c). The vapor phase in the V-type FIs in the quartz-IIa/-IIb is composed primarily of CH_4, N_2 and CO_2 (Fig. 11d). This demonstrates that the Yangla ore fluids were dominantly NaCl-H_2O with varying volatile compositions.

It is worth noting that the vapor compositions in most FIs are dominated by H_2O, but the vapor phases in some quartz FIs contain minor N_2, CO_2, and CH_4,

which may explain why some inclusions did not freeze during cooling or cracked during heating.

4.3 Hydrogen and oxygen isotopes

New and published hydrogen and oxygen isotope data of the Yangla garnet and quartz are listed in Table 3 and illustrated in Figure 12. To calculate the $\delta^{18}O_{fluid}$ values for the garnet, quartz-IIa, and quartz-IIb, we used the average FI homogenization temperatures of 520°C (Lu *et al.*, 1998), 351°C, and 238°C (this study), respectively. The δD and $\delta^{18}O_{fluid}$ values of nine garnets vary from −119.3‰ to −107.8‰ and from 3.9‰ to 8.6‰, respectively. Quartz-IIa have δD values (−137.0 to −101.0‰) similar to those of quartz-IIb (−135.0 to −100.0‰, except for two much higher values obtained by Zhao J.N. 2012). $\delta^{18}O_{fluid}$ values of quartz-IIa (5.7–7.7‰) are higher than those of quartz-IIb (3.0–4.2‰). In the δD versus $\delta^{18}O$ diagram (Fig. 12), the garnet and quartz-IIa data points fall below the primary magmatic water field, whereas the quartz-IIb data points fall in the area between the primary magmatic water field and the meteoric water line.

5. Discussion

5.1 Skarn mineralogy and geochemistry

Based on detailed observations of crosscutting relationships and mineral paragenesis, the chalcopyrite and other sulfides precipitated with quartz and
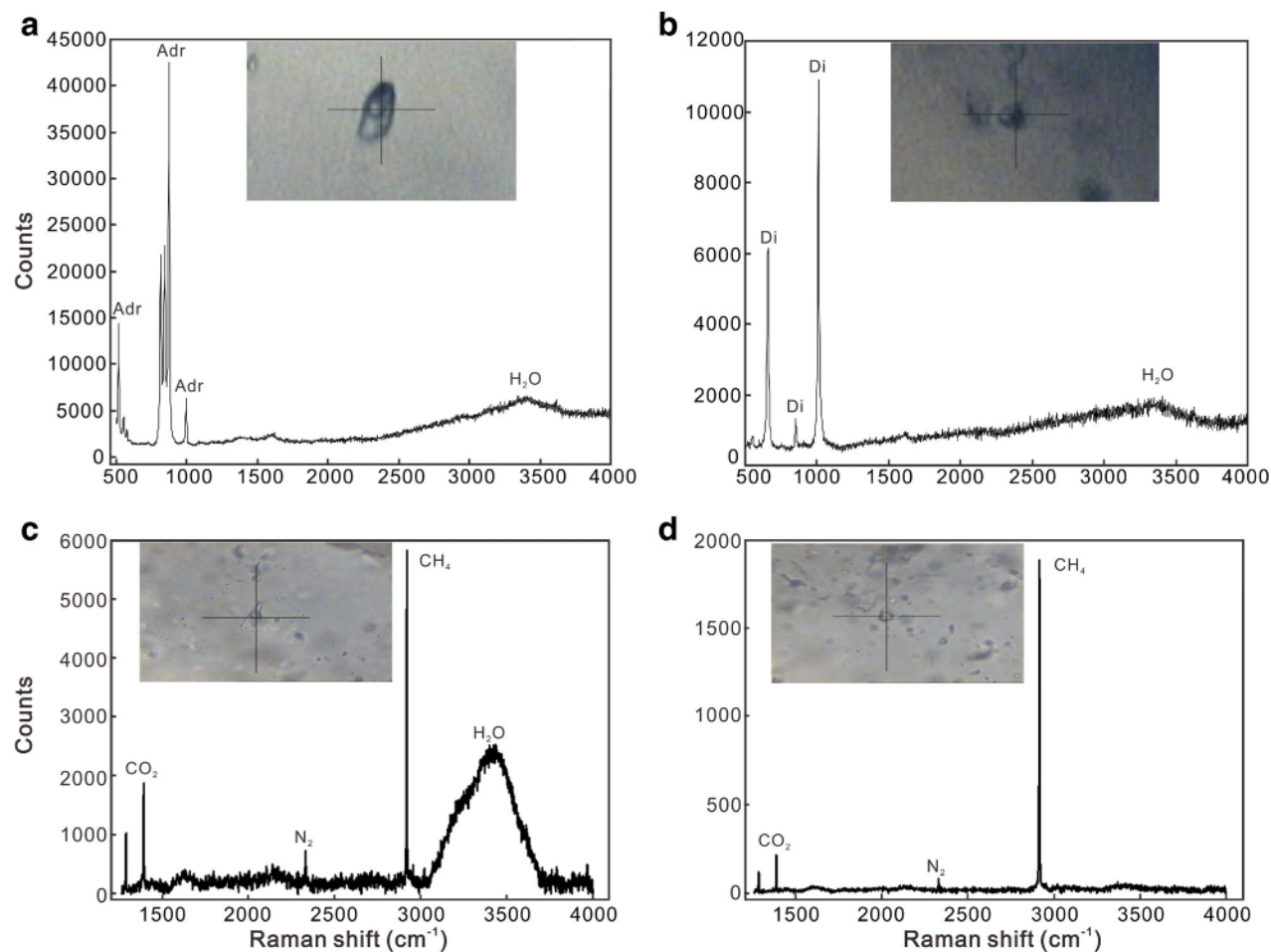
Fig. 11 Representative Raman spectra of fluid inclusions in the Yangla Cu deposit. (a) and (b) H_2O spectra of the vapor phases in the two-phase liquid-rich inclusions in Adr and Di from the pre-ore stage; (c) and (d) H_2O, CO_2, CH_4, and N_2 spectra of vapor phases in the two-phase vapor-rich and two-phase liquid-rich inclusions in quartz from the ore stage. Abbreviations: Adr, andradite; Cal, calcite; Di, diopside; Qz, quartz.

hydrous retrograde alteration minerals, such as epidote and chlorite (Fig. 5d-e, g-h). In addition, the well-developed replacement and fracture-filling textures within the anhydrous calc-silicates and the coexistence of sulfides and stage II hydrous calc-silicates indicate that sulfide mineralization occurred mainly in the retrograde alteration, consistent with most skarn Cu deposits (Meinert *et al.*, 2005). The major orebodies, such as KT2-1, KT2-2, and KT5, are located in the skarn alteration zone, which is another support for the skarn-type metallogenesis at Yangla.

Skarn minerals record the physicochemical conditions during the ore fluid evolution (e.g. Bin & Barton, 1988; Jamtveit *et al.*, 1993; Chapman & Williams, 1998; Clechenko & Valley, 2003; Karimzadeh Somarin, 2010; Stowell *et al.*, 2011; Xu *et al.*, 2015). In

particular, the chemical compositions of garnet and clinopyroxene can indicate the fluid redox state during the skarn alteration (e.g. Einaudi, 1982; Zaw & Singoyi, 2000; Lu *et al.*, 2003; Markowski *et al.*, 2006; Maher, 2010; Oyman, 2010). The Yangla andraditic garnet and diopsidic pyroxene mineral assemblages contain major element geochemistry similar to those from many other Cu skarn deposits (Nakano *et al.*, 1994; Meinert *et al.*, 1997; Meinert *et al.*, 2005) and indicate a relatively high oxygen fugacity (*f*O_2) in the stage I hydrothermal fluids (Table 1; Fig. 7). The high fluid *f*O_2 is also supported by the greater amount of garnet than pyroxene (Meinert *et al.*, 2005; Xu *et al.*, 2015), which is also consistent with most Cu skarn deposits around the world (Meinert *et al.*, 2005). In addition, the local replacement of andradite by

Table 3 Hydrogen-oxygen isotope compositions of the Yangla Cu deposit (‰)

Sample no.	Minerals	δD_{SMOW} (‰)	$\delta^{18}O_{SMOW}$ (‰)	Temperature (°C)	$\delta^{18}O_{fluid}$ (‰)	Data source
3250–46	Garnet	−107.8	4.8	520	7.7	This paper
3250–47	Garnet	−112.5	5.7	520	8.6	This paper
3250–48	Garnet	−115.6	2.6	520	5.5	This paper
3250–49	Garnet	−119.3	2.8	520	5.7	This paper
3250–50	Garnet	−110.6	5.5	520	8.4	This paper
3250–51	Garnet	−109.4	1.5	520	4.4	This paper
3250–52	Garnet	−115.7	2.7	520	5.6	This paper
3250–54	Garnet	−113.6	1.0	520	3.9	This paper
3250–60	Garnet	−114.0	2.0	520	4.9	This paper
YK017-1	Quartz-IIa	−111.0	11.5	351	5.9	This paper
YK018-1	Quartz-IIa	−101.0	12.9	351	7.3	This paper
YK019-1	Quartz-IIa	−118.0	10.9	351	5.3	This paper
LC4	Quartz-IIa	−137.0	13.3	351	7.7	This paper
3904–654	Quartz-IIb	−128.0	12.2	238	2.7	This paper
3250-KT2-4	Quartz-IIb	−135.0	13.7	238	4.2	This paper
3250-KT2-5	Quartz-IIb	−124.0	12.7	238	3.2	This paper
3250-KT2-1	Quartz-IIb	−123.0	12.2	238	2.7	This paper
3250CM-2	Quartz-IIb	−134.0	12.6	238	3.1	This paper
3250CM-8	Quartz-IIb	−134.0	12.3	238	2.8	This paper
3250-8-1-3	Quartz-IIb	−117.0	11.6	238	2.1	This paper
3275	Quartz-IIb	−131.0	11.9	238	2.4	This paper
Feb-75	Quartz-IIb	−133.0	12.3	238	2.8	This paper
L-1	Quartz-IIb	−103.1	10.7	230	0.7	1
L-2	Quartz-IIb	−78.1	11.1	250	2.2	1
L-6	Quartz-IIb	−76.2	11.6	250	2.7	1
YL-8	Quartz-IIb	−104.0	11.6	233	1.8	2
YL-24	Quartz-IIb	−100.0	11.5	249	2.5	2
YL-39	Quartz-IIb	−105.0	10.6	240	1.2	2
YL-40	Quartz-IIb	−115.0	11.9	223	1.5	2
YL-41	Quartz-IIb	−109.0	11.7	212	0.7	2
YL-57	Quartz-IIb	−120.0	11.2	165	−3.0	2

Oxygen isotope fractionations: andradite–water, quartz–water (Zheng, 1993). Data sources: 1-(Zhao, 2012); 2-(Yang, 2012).

hedenbergite suggests decreasing fluid fO_2 with decreasing temperature (Zhu *et al.*, 2015).

The hydrothermal fluid temperatures of stages I and II can be estimated from the mineral assemblages (Einaudi *et al.*, 1981; Meinert, 1992; Meinert, 1998). The Yangla prograde skarn is dominated by garnet, diopside, and hedenbergite, but wollastonite is absent, which indicates a fluid temperature of 430–550°C (Einaudi *et al.*, 1981; Meinert, 1992; Meinert, 1998). This inferred temperature is consistent with the homogenization temperatures of FIs in garnet and clinopyroxene (Zhan *et al.*, 1998; this study).

5.2 Source of ore-forming fluids and materials

Previous studies showed that the Jiaren granitoids are I-type with a crust–mantle mixed origin and are coeval (ca. 230 Ma: zircon U–Pb data by Gao *et al.*, 2010; Zhu et al. 2011) with the Yangla Cu mineralization (molybdenite Re-Os age: ca. 232 Ma; Yang *et al.*, 2012; Zhu *et al.*, 2015). Zhu *et al.* (2015) presented the diagrams of Y versus Nb and Rb versus (Nb + Y), both showing that the Jiaren granitoid is similar to those of the most Cu skarn ore-causative plutons worldwide (Meinert *et al.*, 2005). This, and the fact that stratiform/lenticular skarn orebodies at Yangla are mostly located along the exocontact of the Jiaren granitoid intrusions, further supports the metallogenic link between the Jiaren granitoid and the Yangla Cu mineralization.

The garnet and quartz-IIa samples have lower δD_{fluid} (−137.0‰ to −101.0‰) and $\delta^{18}O_{fluid}$ (3.9–8.6‰) values (Table 3) than primary magmatic water, which is probably led by open-system magma
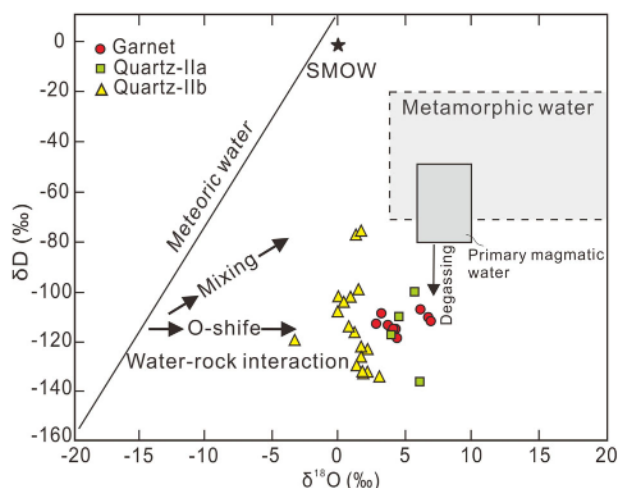
Fig. 12 δD vs. δ^{18}O diagram of the ore fluids in the Yangla Cu deposit. The metamorphic water field, primary magmatic water field, and meteoric water line are obtained from Taylor and Sheppard (1986). Abbreviation: SMOW, standard mean ocean water.

degassing (Taylor & Sheppard, 1986) and water–rock interactions between the hydrothermal fluids and the country rock, respectively. In the δD versus δ^{18}O diagram (Fig. 12), these samples plot below the primary magmatic water field and are slightly closer to the meteoric water line. The quartz-IIb samples yielded a wide δD$_{fluid}$ range (mainly −135 to −100‰) and low δ^{18}O$_{fluid}$ values (−3.0 to 4.2‰; Table 3), which plot in the area between the primary magmatic water field and the meteoric water line (Fig. 12). This suggests meteoric water incursion into the hydrothermal system during stage IIb. Therefore, the hydrogen–oxygen isotope results indicate a predominantly magmatic origin for the Yangla ore fluids with stage IIb meteoric water incursion. This conclusion is further supported by the published near-zero δ^{34}S values (−1.8 to 1.8‰) of the Yangla chalcopyrite (Zhu *et al.*, 2015) and the C-O isotopic compositions of syn-ore stage calcites (δ^{13}C$_{PDB}$ = −7.0‰ to −2.3‰; δ^{18}O$_{SMOW}$ = 10.7–19.4‰; Du *et al.*, 2017). The lead isotope compositions of the Yangla pyrite, pyrrhotite, and chalcopyrite are relatively homogeneous (^{206}Pb/^{204}Pb = 18.273–18.369, ^{207}Pb/^{204}Pb = 15.627–15.677, and ^{208}Pb/^{204}Pb = 38.445–39.611; Zhan *et al.*, 1998) and are broadly comparable with those of the Jiaren granitoids (ca. 230 Ma: zircon U–Pb data by Gao *et al.*, 2010; Zhu et al. 2011) and Devonian Jiangbian and Linong Formations but are distinct

from those of the Carboniferous basalts in the Yangla ore field (Zhu *et al.*, 2015). Therefore, the granitic magma and host rocks may have contributed most of the lead and ore-forming metals (Zhu *et al.*, 2015). Thus, the new H-O isotope and published C-O isotope data indicate that the ore fluids were predominantly of magmatic origin and included some meteoric water at the late syn-ore stage. Besides, S-Pb isotope data all suggest the granitic magma and host rocks contributed most of the lead and ore-forming metals (Zhu *et al.*, 2015).

5.3 Characteristics and evolution paths of the ore-forming fluids

As the Jiaren granitoid pluton cooled and crystallized, an initial fluid with medium-salinity (6–8 wt.% NaCl) and high-temperature (generally approximately 600°C) supercritical fluids and their concentration in the carapace of the magma chamber (Burnham, 1979; Candela, 1989a; Candela, 1989b; Yang & Bodnar, 1994; Bodnar, 1995; Meinert *et al.*, 1997; Robb, 2005). This initial ascent of supercritical fluid to higher levels was likely coincident with the intrusion of the Jiaren granitoids to a depth of approximately 2–3 km beneath the paleosurface (Meinert *et al.*, 1997; Meinert *et al.*, 2003; Zhu *et al.*, 2015). During the initial fluid ascent, a pressure of 50 MPa and a temperature of approximately 500–600°C caused this fluid to boil and separate into a hypersaline liquid phase (approximately 50 wt.% NaCl eqv.; Table 2; Fig. 9) in equilibrium with a lower-density vapor phase. These processes were recorded by FIs that were trapped in the prograde skarn minerals (garnet and clinopyroxene). This phenomenon is consistent with the findings for most Cu skarn deposits, where prograde skarn was formed from this type of hypersaline liquid (Meinert *et al.*, 1997; Meinert *et al.*, 2003). During the separation of the liquid and vapor phases, most of the SO$_2$ and HCl escaped from the initial fluid into the vapor phase, producing a hypersaline liquid with high base metal solubilities and a relatively low sulfur content (Bodnar, 1995; Meinert *et al.*, 2003). This process likely explains the lack of sulfide deposition during the prograde skarn alteration.

As the underlying granitic magma chamber continued to cool and crystallize, a fluid with a composition of bulk Na-K-Cl composition similar to that of the earlier stage fluid may have continually exsolved (Meinert *et al.*, 1997; Meinert *et al.*, 2003). However, this later-ascending fluid did not boil probably

because of lower fluid flux as the parent granitic magma approached the end stages of stagnant crystallization (Meinert *et al.*, 1997; Shinohara & Hedenquist, 1997; Meinert *et al.*, 2003). When the temperature had decreased to less than 400°C, the rock deformation changed from ductile to brittle, resulting in the change from lithostatic to hydrostatic conditions (Fournier, 1992). Therefore, when this later fluid had ascended to approximately 2 km, the pressure was 20 MPa, and the fluid boiled at a temperature of approximately 350°C (average temperature of the quartz-IIa FIs), which led to phase separation of the liquid and vapor. Based on the FI and mineralogical evidence, the quartz and other retrograde alteration minerals, such as epidote and chlorite, formed from this cooler (301–415°C, average 351°C) and less saline (2.6–11.7 (average 7.5) wt.% NaCl eqv.) fluid (Table 2). These conditions accompanied the retrograde alteration and abundant sulfide ore formation.

The stage IIb quartz and calcite vein/veinlets contain FI assemblages with lower salinities (quartz: 1.7–8.1 (average 4.4) wt.% NaCl eqv.; calcite: 1.4–4.8 (average 2.7) wt.% NaCl eqv.) and lower homogenization temperatures (quartz: 165–294°C, average 238°C; calcite: 142–283°C, average 185°C) than those of the stage IIa (Table 2; Fig. 9). Although the fluid-mixing trends in the FIs from the stage IIb are unclear, calculations based on the calcite C-O isotope (Du *et al.*, 2017) and quartz H-O isotope data suggest that meteoric water contributed to the dilution of the ore fluid and triggered the precipitation of abundant minerals (Du *et al.*, 2017).

5.4 Possible deposition mechanism and deposit type

Previous experimental studies showed that copper chloride complexes are likely the most important Cu carrier in porphyry systems (Candela & Holland, 1986; Ulrich *et al.*, 2001; Landtwing *et al.*, 2005) and are the predominant species in high-temperature fluids (Liu & McPhail, 2005). The daughter mineral in the Yangla S-type FIs is halite, suggesting that Cu was also likely transported as chloride complexes in the Yangla ore fluids.

As previously described, we found that Type-S (halite-bearing) and Type-V (vapor-rich) FIs coexisted in garnets of the pre-ore stage for the Yangla deposit (Fig. 8a), indicating that primary FIs were captured almost simultaneously when the fluids were boiling. The phase separation of the initial fluid during boiling

produced a high-salinity brine phase and a low-salinity density vapor phase as inferred from Fig. 10 (Meinert *et al.*, 1997). For example, from the pre-ore stage to the early syn-ore stage, the FI type changed from Type-S + Type-V + Type-L (liquid-rich) to Type-V + Type-L with the conduct of mineralization and was accompanied by the disappearance of Type-S FIs, and homogenization temperature and salinity also tended to decrease dramatically (Fig. 10). This proposal is also provided by previous studies that reported the immiscibility between brine and low-salinity vapor, which is evident by the coexistence of Type-S and Type-V inclusions in skarn systems (Roedder, 1971; Ni *et al.*, 2015). In addition, the formation of skarn minerals (e.g. garnet, clinopyroxene, chlorite, actinolite) may cause the consumption of Na^+, K^+, Ca^+, Cl^-, etc. in ore fluids and further led to the salinity reduction of ore fluids (Golmohammadi *et al.*, 2015). Hence, the disappearance of halite-bearing inclusions (Type-S) may be caused by the formation of skarn minerals at the pre-ore stage.

At the early syn-ore stage, the V-type and L-type FIs coexisted in quartz-IIa (Fig. 8g) and were homogenized to a different phase. In the Th versus salinity diagram (Fig. 10), there is a negative homogenization temperature versus salinity correlation for most of FIs. These features suggest that fluid boiling may have occurred in this stage. By comparing the primary FIs in the skarns, we noted that the homogenization temperature and salinity of inclusions decreased dramatically. This phenomenon indicated that the ore fluids evolved from moderate–high temperature, moderate–high salinity conditions to low-temperature, low-salinity conditions from the skarn stage (pre-ore stage) to the quartz-Cu-Mo-Fe sulfides stage (ore stage). Therefore, during the retrograde alteration at Yangla, the fluids may have ascended to approximately 2 km, and the temperature dropped to just below 400°C, triggering the transition from hypersaline brines emplaced at lithostatic pressure to lower-salinity boiling fluids at hydrostatic pressure (Meinert *et al.*, 1997). This may have resulted in the deposition of most metal sulfides at this stage.

In addition, we also identified Type-L inclusions (liquid-rich) in the late syn-ore stage quartz (Fig. 8h) and calcite (Fig. 8i) from the Yangla deposit. In the Th versus salinity diagram (Fig. 10), the salinities of FIs in quartz and calcite fall within a narrow range with the homogenization temperature drop. The possible mechanisms explaining this phenomenon could be the accession of meteoric water and may have caused

fluid cooling at Yangla. As supported by the new H-O isotope (this study) and published C-O isotope data (Du *et al.*, 2017), the meteoric water incursion into the hotter ore fluid at the late syn-ore stage is indicated. Therefore, we propose that the fluid mixing between a high-temperature magmatic fluid and a low-temperature meteoric water may have led to a significant drop in temperature (from 294°C to 142°C), which further caused the formation of Cu-bearing quartz/calcite veins in the late syn-ore stage. Support for this proposal is also provided by experimental studies, which have shown that a significant temperature drop can destabilize and dissociate the metal chloride complexes, leading to massive metal sulfide precipitation (e.g. Ulrich *et al.*, 2001; Liu & McPhail, 2005). This may have been the case for the Yangla deposit as recorded by the cooling trend of the quartz and calcite FIs data in the late syn-ore stage.

As mentioned above, the Yangla deposit has been identified as an intrusion-related Cu deposit in the Jinshajiang tectonic belt. However, as more in-depth studies have been conducted in recent years, "sedimentary exhalative (SEDEX)," "volcanogenic genesis," and "skarn-type" were terms that were consistently put forward to explain the genesis of the Yangla deposit. Previous studies suggested that the formation of skarn was mainly considered to be through magmatic hydrothermal metamorphism, and the typical skarn deposits developed typical hydrous (e.g. epidote, chlorite, and sericite) and unhydrous (e.g. andradite, diopside, and hedenbergite) skarn minerals (Meinert *et al.*, 1997; Meinert *et al.*, 2005; Siahcheshm, 2017). At Yangla, results of this paper show that skarn minerals are dominated by garnet, diopside, and hedenbergite, and copper mineralization is closely associated with retrograde skarn alteration, which is consistent with most skarn Cu deposits (Meinert *et al.*, 2005). The skarn minerals (garnet) at the pre-ore stage in the Yangla yielded a limited range of high δ^{18}O and high δD values, which suggest a magmatic origin. The δ^{18}O and δD isotope compositions of quartz and calcite indicated that the ore fluid of the ore stage was dominated by magmatic water and mixed by a certain amount of meteoric water. In addition, the Rock-Forming Age (granite SIMS zircon U–Pb dating: 233 ± 1.4 Ma and 231.0 ± 1.6 Ma; Zhu *et al.*, 2011a, 2015) were quite nearly equal to the Ore-forming Age (molybdenite Re-Os dating: ca. 232 Ma; Yang *et al.*, 2012; Zhu *et al.*, 2015). More importantly, our geological survey has proved that Cu orebodies are closely associated with

skarn alteration within the Devonian carbonate rocks (Fig. 3). As such, we can conclude that the Yangla Cu deposit is skarn-type deposit, which formed the magmatism–mineralization process during the Indosinian period.

6. Conclusions

The Yangla deposit is best classified as a Cu skarn deposit. The prograde-skarn garnet and clinopyroxene are dominantly andradite and diopside, respectively, and the Cu mineralization is mainly associated with retrograde alteration, consistent with many Cu skarn deposits around the world.

The Yangla Cu mineralization has a close genetic link with the Jiaren granitoids. The hydrogen and oxygen isotopic compositions suggest that the ore fluids were magmatic dominated, with late-stage meteoric water incursion.

As recorded by the FIs in the prograde-skarn garnet and clinopyroxene, fluid boiling may have occurred during the pre-ore stage, separating the fluid into a hypersaline liquid phase and a lower-density vapor phase. These skarn mineral depositions and wall rock alterations may be caused by the disappearance of halite-bearing inclusions (Type-S) and salinity. Fluid boiling may have occurred due to the change from lithostatic to hydrostatic pressure, which triggered the precipitation of abundant quartz-Cu-Mo-Fe sulfides in the early syn-ore stage. At the late syn-ore stage, fluid mixing between a high-temperature magmatic fluid and a low-temperature meteoric water may have led to a significant drop in temperature and caused the deposition of Cu-bearing quartz/calcite veins. Comprehensive research shows the Yangla deposit is a typical skarn-type deposit that is genetically related to Mesozoic magmatism.

Yunnan Copper Group, including Yue-Dong Liu, Li Yin, and Cheng Luo, as well as Drs. Hai-Rui Sun, Ting Gan, and Qing-Wen Zhang from the IGCAS, for their field assistance. Cenozoic Geoscience Editing & Consultancy (Australia) is acknowledged for the language editing service.

References

Bin, Z. and Barton, M. D. (1988) Compositional characteristics of garnets and pyroxenes in contact-metasomatic skarn deposits and their relationship with metallization. Chin. J. Geochem., 7, 329–335. https://doi.org/10.1007/BF02842337

Bodnar, R. J. (1993) Revised equation and table for determining the freezing-point depression of H_2O–NaCl solutions. Geochim. Cosmochim. Acta, 57, 683–684. https://doi.org/10.1016/0016-7037(93)90378-a

Bodnar, R. J. (1995) Fluid-inclusion evidence for a magmatic source for metals in porphyry copper deposits. Mineral. Assoc. Canada Short Course Series, 23, 395–428.

Bodnar, R. J., Lecumberri-Sanchez, P., Moncada, D. and Steele-MacInnis, M. (2014) 13.5 - fluid inclusions in hydrothermal ore deposits A2 – Holland, Heinrich D. In Turekian, K. K. (ed.) Treatise on geochemistry. 2nd edn. Elsevier, Oxford, 119–142.

Burnham, C. W. (1979) Magmas and hydrothermal fluids. In Barnes, H. L. (ed.) Geochemistry of hydrothermal ore deposits. 2nd edn. John Wiley & Sons, New York, NY, 71–136.

Candela, P. A. (1989a) Felsic magmas, volatiles and metallogenesis. Rev. Econ. Geol., 4, 223–233.

Candela, P. A. (1989b) Magmatic ore-forming fluids: Thermodynamic and mass transfer calculations of metal concentrations. Rev. Econ. Geol., 4, 203–221.

Candela, P. A. and Holland, H. D. (1986) A mass transfer model for copper and molybdenum in magmatic hydrothermal systems; the origin of porphyry-type ore deposits. Econ. Geol., 81, 1–19.

Cao, Y., et al. (2015) Geologic, fluid inclusion and stable isotope constraints on mechanisms of ore deposition at the Datuanshan copper deposit, middle-lower Yangtze Valley, eastern China. Acta Geol. Sin., 89, 746–765.

Chapman, L. H. and Williams, P. J. (1998) Evolution of pyroxene-pyroxenoid-garnet alteration at the Cannington Ag-Pb-Zn deposit, Cloncurry District, Queensland, Australia. Econ. Geol., 93, 1390–1405.

Chen, K. X., Wei, J. Q., Yan, D. P. and Fan, Y. H. (1999) A preliminary study of porphyry bodies and related mineralization in Yangla area, Deqin, Western Yunnan. Geol. Miner. Resour. South China, 1–8 (in Chinese with English abstract).

Chen, S. Y., Gu, X. X., Cheng, W. B., Zheng, G., Han, S. Y. and Peng, Y. W. (2013) Characteristics of ore-forming fluid and mineralization process of the Yangla copper deposit, Yunnan. Earth Sci. Frontiers, 20, 82–91 (in Chinese with English abstract).

Clayton, R. N. and Mayeda, T. K. (1963) The use of bromine pentafluoride in the extraction of oxygen from oxides and silicates for isotopic analysis. Geochim. Cosmochim. Acta, 27, 43–52.

Clechenko, C. C. and Valley, J. W. (2003) Oscillatory zoning in garnet from the Willsboro Wollastonite Skarn, Adirondack Mts, New York: A record of shallow hydrothermal processes preserved in a granulite facies terrane. J. Metamorph. Geol., 21, 771–784. https://doi.org/10.1046/j.1525-1314.2003.00478.x

Coleman, M. L., Shepherd, T. J., Durham, J. J., Rouse, J. E. and Moore, G. R. (1982) Reduction of water with zinc for hydrogen isotope analysis. Anal. Chem., 54, 993–995.

da Costa Silva, A. R., Nobre Villas, R. N., Lafon, J.-M., Craveiro, G. S. and Ferreira, V. P. (2015) Stable isotope systematics and fluid inclusion studies in the Cu-Au Visconde deposit, Carajas Mineral Province, Brazil: Implications for fluid source generation. Miner. Deposita, 50, 547–569.

Deng, J., Hou, Z. Q., Mo, X. X., Yang, L. Q., Wang, Q. F. and Wang, C. M. (2010) Superimposed orogenesis and metallogenesis in Sanjiang. Tethys Miner. Deposits, 29, 37–42.

Deng, J., Yang, L. Q. and Wang, C. M. (2011) Research advances of superimposed orogenesis and metallogenesis in the Sanjiang Tethys. Acta Petrol. Sin., 27, 2501–2509.

Deng, J., Wang, C. M. and Santosh, M. (2014a) Orogenesis and metallogenesis in the Sanjiang Tethyan domain, China: preface. Gondwana Res., 26, 415–418. https://doi.org/10.1016/j.gr.2013.12.003

Deng, J., Wang, Q. F., Li, G. J., Li, C. S. and Wang, C. M. (2014b) Tethys tectonic evolution and its bearing on the distribution of important mineral deposits in the Sanjiang region, SW China. Gondwana Res., 26, 419–437.

Driesner, T. and Heinrich, C. A. (2007) The system H2O–NaCl. Part I: Correlation formulae for phase relations in temperature–pressure–composition space from 0 to 1000 °C, 0 to 5000 bar, and 0 to 1 XNaCl. Geochim. Cosmochim. Acta, 71, 4880–4901.

Du, L. J., Li, B., Huang, Z. L., Zhou, J. X., Zou, G. F. and Yan, Z. F. (2017) Carbon-oxygen isotopic geochemistry of the Yangla Cu skarn deposit, SW China: Implications for the source and evolution of hydrothermal fluids. Ore Geol. Rev., 88, 809–821.

Einaudi, M. T. (1982) General features and origin of skarns associated with porphyry copper plutons, Southwestern North America. In Titley, S. R. (ed.) Advances in the geology of porphyry copper deposits. University of Arizona Press, Tucson.

Einaudi, M. T., Meinert, L. D. and Newberry, R. J. (1981) Skarn deposits. In Skinner, B. J. (ed.) Economic Geology 75th Anniversaly Volume. Economic Geology Publishing Company, El Paso, 317–391.

Fournier, R. O. (1992) The influences of depth of burial and the brittle-ductile transition on the evolution of magmatic fluids. Geological Survey Japan Report, 279.

Gao, R., Xiao, L., He, Q., Yuan, J., Ni, P. Z. and Du, J. X. (2010) Geochronology, geochemistry and petrogenesis of granites in Weixi-Deqin, West Yunnan. Earth Sci. J. China Univ. Geosci., 35, 186–200 (in Chinese with English abstract).

Golmohammadi, A., Karimpour, M. H., Shafaroudi, A. M. and Mazaheri, S. A. (2015) Alteration-mineralization, and radiometric ages of the source pluton at the Sangan iron skarn deposit, northeastern Iran. Ore Geol. Rev., 65, 545–563.

Hedenquist, J. W. and Lowenstern, J. B. (1994) The role of magmas in the formation of hydrothermal ore deposits. Nature, 370, 519–527.

Hedenquist, J. W., Arribas, A. and Reynolds, T. J. (1998) Evolution of an intrusion-centered hydrothermal system: far

Southeast-Lepanto porphyry and epithermal Cu-Au deposits. Econ. Geol., 93, 373–404.

Hou, Z. Q. and Zhang, H. R. (2015) Geodynamics and metallogeny of the eastern Tethyan metallogenic domain. Ore Geol. Rev., 70, 346–384. https://doi.org/10.1016/j.oregeorev.2014.10.026

Hou, Z. Q., Ma, H., Zaw, K., Zhang, Y., Wang, M., Wang, Z. W., Pan, G. P. and Tang, R. (2003) The Himalayan Yulong porphyry copper belt: Product of large-scale strike-slip faulting in eastern Tibet. Econ. Geol., 98, 125–145.

Hou, Z. Q., Zaw, K., Pan, G. T., Mo, X. X., Xu, Q., Hu, Y. Z. and Li, X. Z. (2007) Sanjiang Tethyan metallogenesis in SW China: tectonic setting, metallogenic epochs and deposit types. Ore Geol. Rev., 31, 48–87.

Hu, R. Z., Burnard, P. G., Bi, X. W., Zhou, M. F., Pen, J. T., Su, W. C. and Wu, K. X. (2004) Helium and argon isotope geochemistry of alkaline intrusion-associated gold and copper deposits along the Red River-Jinshajiang fault belt, SW China. Chem. Geol., 203, 305–317.

Jamtveit, B., Wogelius, R. A. and Fraser, D. G. (1993) Zonation patterns of skarn garnets: records of hydrothermal system evolution. Geology, 21, 113–116.

Karimzadeh Somarin, A. (2010) Garnetization as a ground preparation process for copper mineralization: evidence from the Mazraeh skarn deposit, Iran. Int. J. Earth Sci. (Geol Rundsch), 99, 343–356.

Landtwing, M. R., Pettke, T., Halter, W. E., Heinrich, C. A., Redmond, P. B., Einaudi, M. T. and Kunze, K. (2005) Copper deposition during quartz dissolution by cooling magmatic-hydrothermal fluids: The Bingham porphyry. Earth Planet. Sci. Lett., 235, 229–243.

Liu, W. H. and McPhail, D. C. (2005) Thermodynamic properties of copper chloride complexes and copper transport in magmatic-hydrothermal solutions. Chem. Geol., 221, 21–39.

Lu, Y. F., Zhan, M. G., Chen, K. X. and Huang, H. L. (1998) Fluid inclusions in ore-bearing skarns from the Yangla copper mineralization concentrated area of Deqen County, Yunnan province. Miner. Deposits, 4, 331–341 (in Chinese with English abstract).

Lu, Y. F., Chen, K. X. and Zhan, M. G. (1999) Geochemical evidence of exhalative-sedimentary ore-bearing skarns in Yangla copper mineralization concentrated area, Deqin county, northwestern Yunnan province. Earth Sci. J. China Univ. Geosci., 24, 298–303 (in Chinese with English abstract).

Lu, H. Z., Liu, Y. M., Wang, C. L., Xu, Y. Z. and Li, H. Q. (2003) Mineralization and fluid inclusion study of the Shizhuyuan W-Sn-Bi-Mo-F skarn deposit, Hunan Province, China. Econ. Geol., 98, 955–974.

Lu, H. Z., Fan, H. R., Ni, P., Ou, G. X., Shen, K. and Zhang, W. H. (2004). Fluid inclusion. Science Press, Beijing, China, 202–229.

Maher, K. C. (2010) Skarn alteration and mineralization at coroccohuayco, Tintaya District, Peru. Econ. Geol., 105, 263–283.

Mai, B. X. and Wang, B. S. (1992) Characteristics and applications of fluid inclusions in the Eogene system of the Biyang depression—I. a fluid inclusion study. Chin. J. Geochem., 11, 370–383.

Markowski, A., Vallance, J., Chiaradia, M. and Fontboté, L. (2006) Mineral zoning and gold occurrence in the Fortuna skarn mine, Nambija district, Ecuador. Miner. Deposita, 41, 301–321.

Meinert, L. D. (1992) Skarn and skarn deposits. Geosci. Can., 19, 145–162.

Meinert, L. D. (1998) A revies of skarns that contain gold. Miner. Assoc. Canada Short Course Series, 26, 359–414.

Meinert, L. D., Hefton, K. K., Mayes, D. and Tasiran, I. (1997) Geology, zonation, and fluid evolution of the big Gossan Cu-Au skarn deposit, Ertsberg district: Irian Jaya. Econ. Geol., 92, 509–534.

Meinert, L. D., Hedenquist, J. W., Satoh, H. and Matsuhisa, Y. (2003) Formation of anhydrous and hydrous skarn in Cu-Au ore deposits by magmatic fluids. Econ. Geol., 98, 147–156.

Meinert, L., Dipple, G. M. and Nicolescu, S. (2005) World skarn deposits. In Hedenquist, J. W., Thompson, J. F. H., Goldfarb, R. J., and Richards, J. P. (eds.) Economoc Geology 100th Annversary Volume. Society of Economoc Geologists Inc., Littleton, 299–336.

Meng, X., Mao, J., Zhang, C., Zhang, D., Kong, Z. and Jia, F. (2016) The timing, origin and T-fO_2 crystallization conditions of long-lived magmatism at the Yangla copper deposit, Sanjiang Tethyan orogenic belt: implications for post-collisional magmatic-hydrothermal ore formation. Gondwana Res., 40, 211–229.

Metcalfe, I. (2013) Gondwana dispersion and Asian accretion: tectonic and palaeogeographic evolution of eastern Tethys. J. Asian Earth Sci., 66, 1–33.

Mo, X. X., et al. (1993). Sanjiang Tethyan volcanism and related mineralization. Geological Publishing House, Beijing.

Moritz, R. (2006) Fluid salinities obtained by infrared micro-thennometry of opaque minerals: Implications for ore deposit modeling - a note of caution. J. Geochem. Explor., 89, 284–287.

Nakano, T., Yoshino, T., Shimazaki, H. and Shimizu, M. (1994) Pyroxene composition as an indicator in the classification of skarn deposits. Econ. Geol., 89, 1567–1580.

Ni, P., Wang, G. G., Yu, W., Chen, H., Jiang, L. L., Wang, B. H., Zhang, H. D. and Xu, Y. F. (2015) Evidence of fluid inclusions for two stages of fluid boiling in the formation of the giant Shapinggou porphyry Mo deposit, Dabie Orogen, Central China. Ore Geol. Rev., 65, 1078–1094.

Oyman, T. (2010) Geochemistry, mineralogy and genesis of the Ayazmant Fe–Cu skarn deposit in Ayvalik,(Balikesir), Turkey. Ore Geol. Rev., 37, 175–201.

Pan, J. Y., Zhang, Q. and Li, C. Y. (2000) REE geochemistry of the Yangla copper deposit in western Yunnan. Acta Miner. Sin., 20, 44–49 (in Chinese with English abstract).

Pan, J. Y., Zhang, Q., Ma, D. S. and Li, C. Y. (2001) Cherts from the Yangla copper deposit, western Yunnan Province: geochemical characteristics and relationship with massive sulfide mineralization. Sci. China Ser. D Earth Sci., 44, 237–244 (in Chinese with English abstract).

Philippot, P. (2015) Fluid inclusions. In Gargaud, M., et al. (eds.) Encyclopedia of astrobiology. Springer, Berlin, 859–863.

Qiu, Z. J., et al. (2015) Fluid inclusion and carbon-oxygen isotope studies of the Hujiayu cu deposit, Zhongtiao Mountains, China: implications for Syn-metamorphic copper remobilization. Acta Geol. Sin., 89, 726–745.

Qu, X. M., Yang, Y. Q. and Li, Y. G. (2004) A discussion on origin of Yangla copper deposit in light of diversity of ore-hosting rock types. Miner. Deposits, 23, 431–444 (in Chinese with English abstract).

Robb, L. (2005) Magmatic-hydrothermal ore-forming processes. In Robb, L. (ed.) Introduction to ore-forming processes. Blackwell, Malden, 75–125.

Roedder, E. (1971) Fluid inclusion studies on the porphyry-type ore deposits at Bingham, Utah, Butte, Montana, and climax, Colorado. Econ. Geol., 66, 98–118.

Roedder, E. and Bodnar, R. J. (1980) Geologic pressure determinations from fluid inclusion studies. Annual Review of Earth and Planetary Sciences, 8: 263–301.

Roedder, E. (1984) Fluid inclusions. Rev. Miner., 12, 644 p.

Rusk, B. G., Reed, M. H. and Dilles, J. H. (2008) Fluid inclusion evidence for magmatic-hydrothermal fluid evolution in the porphyry copper-molybdenum deposit at Butte, Montana. Econ. Geol., 103, 307–334. https://doi.org/10.2113/gsecongeo.103.2.307

Shinohara, H. and Hedenquist, J. W. (1997) Constraints on magma degassing beneath the far southeast porphyry cu-au deposit, Philippines. J. Petrol., 38, 1741–1752.

Siahcheshm, K. (2017) Mineralogy and metasomatic evolution of the Mianeh iron skarn deposit, Norduz-Agarak border, NW Iran. Arab. J. Geosci., 10, 309.

Stefanova, E., Driesner, T., Zajacz, Z., Heinrich, C. A., Petrov, P. and Vasilev, Z. (2014) Melt and fluid inclusions in hydrothermal veins: The magmatic to hydrothermal evolution of the Elatsite porphyry cu-au deposit, Bulgaria. Econ. Geol., 109, 1359–1381.

Stowell, H., Zuluaga, C., Boyle, A. and Bulman, G. (2011) Garnet sector and oscillatory zoning linked with changes in crystal morphology during rapid growth, north cascades, Washington. Amer. Miner., 96, 1354–1362.

Taylor, H. P. and Sheppard, S. M. (1986) Igneous rocks; I, processes of isotopic fractionation and isotope systematics. Rev. Miner. Geochem., 16, 227–271.

Ulrich, T., Gunther, D. and Heinrich, C. A. (2001) The evolution of a porphyry Cu-Au deposit, based on LA-ICP-MS analysis of fluid inclusions: Bajo de la Alumbrera, Argentina. Econ. Geol., 96, 1743–1774.

Wang, X. F., Metcalfe, I., Jian, P., He, L. Q. and Wang, C. S. (2000) The Jinshajiang-Ailaoshan suture zone, China: Tectonostratigraphy, age and evolution. J. Asian Earth Sci., 18, 675–690. https://doi.org/10.1016/s1367-9120(00)00039-0

Wang, B. D., Wang, L. Q., Chen, J. L., Yin, F. G., Wang, D. B., Zhang, W. P., Chen, L. K. and Liu, H. (2014) Triassic three-stage collision in the Paleo-Tethys: constraints from magmatism in the Jiangda-Deqen-Weixi continental margin arc, SW China. Gondwana Res., 26, 475–491. https://doi.org/10.1016/j.gr.2013.07.023.

Wei, J. Q., Zhan, M. G., Lu, Y. F., Chen, K. X. and He, L. Q. (1997) Geochemistry of granitoids in Yangla ore district, western Yunnan. Geol. Miner. Resour. South China, 13, 50–56 (in Chinese with English abstract).

Wilkinson, J. J. (2010) A review of fluid inclusion constraints on mineralization in the Irish ore field and implications for the genesis of sediment-hosted Zn-Pb deposits. Econ. Geol., 105, 417–442.

Xiao, L., Qi, H., Pirajno, F., Ni, P. Z., Du, J. X. and Wei, Q. R. (2008) Possible correlation between a mantle plume and the evolution of Paleo-Tethys Jinshajiang Ocean: evidence from a volcanic rifted margin in the Xiaru-Tuoding area, Yunnan, SW China. Lithos, 100, 112–126.

Xu, Y. M., Jiang, S. Y., Zhu, Z. Y. and Zhou, W. (2015) Mineral chemistry and H-O-S-Pb isotopic compositions of skarn type copper deposits in the Jiurui district of the Middle-Lower Yangtze River metallogenic belt, Eastern China. Ore Geol. Rev., 69, 88–103.

Yang, X. A. (2012) Superimposition mineralization and exploring model in the Yangla metallogenic belt, western Yunnan. Ph.D. thesis, China University of Geosciences (Beijing).

Yang, K. and Bodnar, R. J. (1994) Magmatic-hydrothermal evolution in the "bottoms" of porphyry copper systems: Evidence from silicate melt and aqueous fluid inclusions in granitoid intrusions in the Gyeongsang basin, South Korea. Int. Geol. Rev., 36, 608–628.

Yang, X. A., Liu, J. J., Cao, Y., Han, S. Y., Gao, B.-y., Wang, H. and Liu, Y. D. (2012) Geochemistry and S, Pb isotope of the Yangla copper deposit, western Yunnan, China: implication for ore genesis. Lithos, 144, 231–240.

Zaw, K. and Singoyi, B. (2000) Formation of magnetite-scheelite skarn mineralization at Kara, northwestern Tasmania: Evidence from mineral chemistry and stable isotopes. Econ. Geol., 95, 1215–1230.

Zaw, K., Peters, S. G., Cromie, P., Burrett, C. and Hou, Z. (2007) Nature, diversity of deposit types and metallogenic relations of South China. Ore Geol. Rev., 31, 3–47. https://doi.org/10.1016/j.oregeorev.2005.10.006

Zhan, M. G., et al. (1998). Yangla copper deposit in Deqin, western China. China University of Geoscience Publishing House, Wuhan.

Zhang, Y. M., Gu, X. X., Liu, L., Dong, S. Y., Li, K., Li, B. H. and Lv, P. R. (2011) Fluid inclusion and H-O isotope evidence for immiscibility during mineralization of the Yinan Au-Cu-Fe deposit, Shandong, China. J. Asian Earth Sci., 42, 83–96.

Zhang, F. F., Wang, Y.-H. and Liu, J.-J. (2016) Fluid inclusions and H–O–S–Pb isotope systematics of the Baishan porphyry Mo deposit in Eastern Tianshan, China. Ore Geol. Rev., 78, 409–423.

Zhao, J. N. (2012) Geological and geochemical characteristics of ore body and deep ore exploration from Yangla ore deposit, Western Yunnan (Ph.D. Thesis). China University of Geosciences, Wuhan, pp. 1–147 (in Chinese with English abstract).

Zheng, Y. F. (1993) Calculation of oxygen isotope fractionation in anhydrous silicate minerals. Geochim. Cosmochim. Acta, 57, 1079–1079.

Zhu, J., et al. (2011a) Geological and geochemical evidences of compound genesis of Yangla bedded copper deposit, northwestern Yunnan. Geol. Rev., 57, 337–349 (in Chinese with English abstract).

Zhu, J. J., Hu, R. Z., Bi, X. W., Zhong, H. and Chen, H. (2011b) Zircon U-Pb ages, Hf-O isotopes and whole-rock Sr-Nd-Pb isotopic geochemistry of granitoids in the Jinshajiang suture zone, SW China: constraints on petrogenesis and tectonic evolution of the Paleo-Tethys Ocean. Lithos, 126, 248–264.

Zhu, J. J. (2012) The geological setting and metallogenesis of the Yangla copper deposit, SW Yunnan (Ph.D. Thesis). Institute of Geochemistry, Chinese Academy of Sciences, Guiyang, pp. 1–178 (in Chinese with English abstract).

Zhu, J. J., Hu, R. Z., Richards, J. P., Bi, X. W. and Zhong, H. (2015) Genesis and magmatic-hydrothermal evolution of the Yangla skarn Cu deposit, Southwest China. Econ. Geol., 110, 631–652.